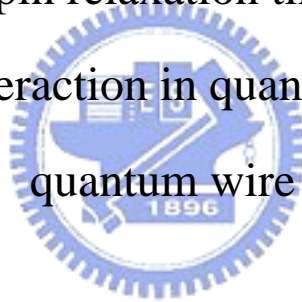


國立交通大學
電子物理研究所
碩士論文

量子點中電子與環境聲子交互作用探討

Study on spin relaxation time due to the
electron-phonon interaction in quantum dot embedded in
quantum wire



研究生:陳柏文

Student: Po-Wen Chen

指導教授:褚德三博士

Advisor: Der-San Chuu

中華民國九十四年七月

量子點中電子與環境聲子交互作用探討

Study on spin relaxation time due to the electron-phonon
interaction in quantum dot embedded in quantum wire

研究生:陳柏文

Student: Po-Wen Chen

指導教授:褚德三

Advisor: Der-San Chuu

國立交通大學



Submitted to Institute of Electrophysics

College of Science

National Chiao Tung University

In Partial Fulfillment of the Requirments

For the Degree of Master of Science in Electrophysics

August 2004

Hsinchu, Taiwan, Republic of China

中華民國九十四年七月


量子點中電子與環境聲子交互作用探討

學生：陳柏文

指導教授：褚德三

國立交通大學電子物理研究所

摘要



在本論文中，我們主要考慮量子點限制在一維量子線結構中，研究量子點中自旋弛豫時間。自旋弛豫時間是由於量子點電子與環境的聲子(一維量子線)交互作用的產生，並且用 Fermi golden rule 的方法去計算量子點和環境聲子的交互作用中自旋弛豫時率，我們探討不同的磁場強度，量子點的大小與溫度高低，量子線(quantum wire)的長寬大小對自旋弛豫時間的影響。

Study on spin relaxation time due to the electron-phonon interacting in quantum dot embedded in quantum wire.

Student : Po-Wen Chen

Advisor : Der-San Chuu

Institute of Electrophysics
National Chiao-Tung University

Abstract



In this thesis, we investigate the spin relaxation time in quantum dot embedded into quantum wire. The spin relaxation time due to the electron-phonon interaction is studied. We calculate spin relaxation time by Fermi golden rule. Different effects such as the magnetic field, the quantum dot size, and the temperature on the spin relaxation time are studied.

誌 謝

此篇論文能夠順利完成，首先要感謝指導教授褚德三博士，儘管繁重的教學與研究工作忙碌，老師也無法移開對學生的關注，每當學生陷於苦思時，老師總是能適時地指導並給予獨到的見解，讓學生收益良多，我將銘記在心。老師待人開朗健談，更是學生學習的榜樣。論文撰寫期間，謝謝老師耐心的諄諄教誨，口試期間還要感謝口試委員江進福老師、楊賜麟老師及周武清老師的詳細審閱以及寶貴的指正與建議，使論文得以更臻完備，在此獻在最深的謝意。

另外，還要謝謝我的實驗室學長岳男、英彥、高進、哲明、裕煌、英讚、瑞雯、詩衍、敏男以及學弟們，感謝學長們的協助與討論開啟我對物理領域的興趣，電腦上所給予的支援令我感激及生涯上的分享，讓我視野開拓，得以更詳盡的規劃人生，在此獻上無限的感激。

還要謝謝我的研究所同學—政益、詩雯，在求學階段相互幫忙鼓勵，更讓我在研究所期間增添許多美好的歡樂回憶。還有我的大學同窗摯友瑋駿、裕善、宇久、士中的加油打氣，以及女友曉佩的關心與勉勵，讓我得以積極勇敢的邁向人生中各個關卡。

最後要感謝我的家人，感謝他們在我研究期間對我的鼓勵與精神上的支持。使我可以在沒有顧慮的情況下，專心研究問題、完成學位。

要感謝的人很多，掛一漏萬，若有遺漏在此也一併獻上內心最深的謝意。

List of Figures

Fig.1 The cylindrical-shaped quantum dot in an applied magnetic field.

Fig.2 For a cubic medium , volume of cube is $\Delta x \Delta y \Delta z$

Fig.3 A rectangular rod of infinite length in z-direction with a height 2a in x-direction and a width 2d in the y-direction.

Fig.4 Energy levels for quantum dot with an effective diameter $d=20$ nm and $d=40$ nm , spin orbit coupling is not included , at least 12-levels

$|0,0,\uparrow\rangle, |0,0,\downarrow\rangle, |0,1,\uparrow\rangle, |0,1,\downarrow\rangle, \dots, |1,1,\downarrow\rangle, |1,-1,\uparrow\rangle, |1,-1,\downarrow\rangle$

are included.

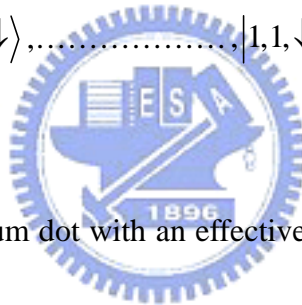


Fig.5 Energy levels for quantum dot with an effective diameter $d=10$ nm, $d=20$ nm, respectively with including Dressshauls effective interaction.

Fig.6 Energy levels for quantum dot with an effective diameter $d=30$ nm , $d=40$ nm, respectively with including Dressshauls effective interaction.

Fig.7 Energy levels for quantum dot with an effective diameter $d=50$ nm, $d=60$ nm , respectively with including Dressshauls effective interaction.

Fig.8 For $d=60$ nm, 12 and 24 basis functions are included in order to obtain a convergence of the lowest 2 levels and ensure the 0.15% precision with 24 basis functions.

Fig.9 The corresponding energy splitting ΔE between the lowest two levels for $d=20\text{nm}, d=30\text{nm}, d=40\text{nm}, d=50\text{nm},$ and $d=60\text{nm}$. Anticrossing levels occur at $B=0.45\text{T}, 0.67\text{T}, 1.1\text{T}, 1.8\text{T}, 4.02\text{T}$ for $d=60\text{nm}, d=50\text{nm}, d=40\text{nm}, d=30\text{nm}, d=20\text{nm}$, respectively.

Fig.10 Dispersion curves for the six lowest width and thickness modes of a $130\text{nm} \times 260\text{nm}$ quantum wire.

Fig.11 Dispersion curves for the six lowest width and thickness modes of a $100\text{nm} \times 200\text{nm}$ quantum wire.

Fig.12 Magnitude effect of Dresshaus's interaction for a quantum dot embedded in a quantum wire.

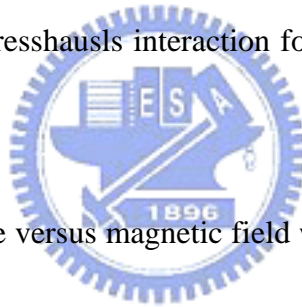


Fig.13 The spin relaxation rate versus magnetic field with the size of the quantum dot in a range of $d=20 \sim d=60\text{nm}$ at temperature $T=10\text{K}$ and 4K .

Fig.14 The spin relaxation rate versus magnetic field for various temperatures $T=10\text{K}$ 、 $T=4\text{K}$ 、 $T=2\text{K}$ and the size of the quantum dot are kept at $d=20$ 、 $d=40\text{nm}$.

Fig.15 The spin relaxation time versus temperature under different magnetic field at $d=30\text{nm}$ and $d=50\text{nm}$.

Fig.16 (a) The SRT versus the width of the quantum wire in different quantum dot diameters at $B=1\text{T}$. (b) The SRT versus the width of the quantum wire in different temperatures at $d=20\text{nm}$.

Contents

Figure Captions

Chapter 1 Introduction	9
Chapter 2 Formulation	12
2.1 quantum dot.....	12
2.2 acoustic phonon.....	18
2.3 electron-phonon interaction.....	22
Chapter 3 Results and Discussions.....	27
Chapter 4 Conclusions.....	31
Appendix A.....	33
Appendix B.....	41
Appendix C.1.....	47
Appendix C.2.....	48
References.....	50

Chapter 1

Introduction

Quantum dot is a small conductive region in semiconductor structures. The size of the quantum dots can be controlled by gate voltage [1] [20]. Quantum dot can be defined as a solid-state structure capable of confining the electrons. [2][26] Quantum information indicated that the state of an electron spin $1/2$ can be encode quantum information in a semiconductor quantum dot. [3]. However, information processing is intrinsically limited by the spin lifetime. For a single spin, one distinguishes between two characteristic decay times T_1 and T_2 , where T_1 is the spin-relaxation time and T_2 is the spin decoherence time. The relaxation of an excited spin state in a magnetic field into the thermal equilibrium is associated with the spin-relaxation time T_1 . The spin decoherence time T_2 is related to the loss of phase coherence of a single spin that is prepared in a superposition of its eigenstates. [4] Experimentally, T_2 measurements of a single spin in quantum dot are highly desirable because T_2 is the limiting time scale for the coherent spin manipulation [4]. Spontaneous emission is one of the fundamental concepts of quantum mechanics that can be traced back to the early work of Albert Einstein. [3] An excited state of a single atom decays

exponentially due to the coupling to phonon. If the quantum dot with discrete bare levels is coupled to external degree of freedom, these levels will acquire a finite width Γ . [4][21][22] The properties of electron-spins confined in semiconductor quantum dot are essential to the proposed qubits in quantum computers. The study of spin relaxation in quantum dot is implemented with the search for solid state qubits in quantum information. It needs to obtain longer spin coherence time so that quantum information can be stored and manipulated without losses. [5-9].

Spin-orbit interaction in semiconductors is essential in spin relaxation processes because phonons alone do not flip spins. Spin relaxation in quantum dots can arise from acoustic phonon-assisted spin flips at low temperatures.[5][20][25] The dominant factors on the spin relaxation processes are the dot size, temperature, and magnetic field . Low temperature relaxation rates are found to be small and to depend strongly on the size and temperature of the dot, and is also dependent on the magnetic field applied on the dot. [1][10-13]

Recently, an increasing interest in the spin properties of nanostructure has been found. In this work, we calculate the relaxation time of spin flip due to the spin-orbit coupling induced spin-flip electron-phonon scattering at very low temperatures, where the dominant electron-phonon scattering arises from the deformation potential[14]. The study of spin relaxation time is usually by the perturbation theory where the

spin-orbit coupling is treated as a perturbation in the Hilbert space spanned by H_0 which does not include the spin-orbit coupling [2][15-16]. We investigate the spin relaxation time (SRT) of GaAs quantum dot confined by parabolic confining potentials and is embedded in a rectangular quantum wire. Our system is solved by exactly diagonalizing the total Hamiltonian. We then calculate the SRT due to the scattering with the acoustic phonons by Fermi golden rule after the energy levels and wave functions are obtained from the exact diagonalization [17-19] [30]. In this thesis, we study the effects of the magnetic field, the temperature, and the quantum wire width (thickness) on the SRT. [31-40]



Chapter 2

Formulation

2.1 quantum dot

Consider a system consisting of an electron in a cylindrical quantum dot acted by an external magnetic field, the quantum dot is embedded in a rectangular waveguide (quantum wire) and is interacted with acoustic phonon inside the quantum wire.

The Hamiltonian of the system is:

$$H = H_e + H_{ph} + H_{e-ph} \quad (2.1.1)$$

where $H_e = H_o + H_{so}$ (2.1.2)

H_o is the electron Hamiltonian without the spin-orbit coupling (Dresshauls effect) and can be expressed as :

$$H_o = \frac{p^2}{2m^*} + V_c(r) + H_B \quad (2.1.3)$$

The first term of H_o is the kinetic energy operator i.e $p = -i\hbar\nabla + \frac{e}{c}\bar{A}$,

with $\bar{A} = \frac{1}{2}(B \times r)$.

The second term is the confining potential $V_c(r) = \hbar\omega_o = \frac{\hbar^2}{m^*d^2}$, where d

is the effective diameter and m^* is the electron effective mass. The third term

$H_B = \frac{1}{2}gu_B B\sigma_z$ is the Zeeman energy, where g is the g-factor (here we will

consider a GaAs quantum dot, thus $g = -0.44$), $\mu_B = \frac{e\hbar}{2m}$ is the Bohr magneton, and σ_z is the z component of Pauli matrix.

The SO interaction H_{so} is comprised of the two parts (Dresshauls and Rashba terms). The Rashba (Electric field) and Dresshauls (Strain field) SO Hamiltonians may be written as

$$H_{so} = \alpha (-P_x \sigma_x + P_y \sigma_y) + \beta (\sigma_x p_y - p_y \sigma_x) \quad (2.1.4)$$

By (2.1.4), the second term is neglected because strain field (Dresshauls term) is only considered, H_{so} can be simplified as

$$H_{so} = \alpha (-P_x \sigma_x + P_y \sigma_y) \quad (2.1.5)$$

, in which $\alpha = \alpha_c \pi^2 (\frac{1}{a^2})$, $\alpha_c = 27.5 \text{ \AA}^3 \text{-eV}$.

H_{ph} contained in eq.(2.1.1) can be express as (Appendix C.1) and we only consider the acoustic phonon.

$$H_{ph} = \hbar \omega_q (a_q^\dagger a_q + \frac{1}{2}) \quad (2.1.6)$$

, where $\hbar \omega_q$ is the acoustic phonon energy, a_q^\dagger and a_q are the creation and annihilation operator for acoustic phonon.

The electron-phonon interaction between the electron in quantum dot and the acoustic phonon in quantum wire can be expressed as (Appendix C.2)

$$H_{ep} = \sum_q M_q (a_q^\dagger + a_q) e^{iq \cdot r} \quad (2.1.7)$$

with M_q being the scattering matrix form.

The wavefunction of the electron in quantum dot $|\psi_I\rangle$ (i.e. the state function of the Hamiltonian H_e in the Hilbert Space) can be constructed from the eigenfunction functions $|\mathbf{n} \ l \ \sigma\rangle$ of H_o without spin-orbital interaction as

$$|\psi_I\rangle = \sum_{nl\sigma} C_{nl\sigma}^I |\mathbf{n} \ l \ \sigma\rangle \quad (2.1.8)$$

, here $H_o |\mathbf{n} \ l \ \sigma\rangle = E_{nl\sigma} |\mathbf{n} \ l \ \sigma\rangle$ with

$$|\mathbf{n} \ l \ \sigma\rangle = R_{nl} e^{i l \theta} \chi_\sigma = \sqrt{\left[\frac{\alpha^2 \mathbf{n}!}{\pi(n+|l|)!} \right]} (\alpha r)^{|l|} \exp\left(-\frac{(\alpha r)^2}{2}\right) L_n^{|l|}(\alpha^2 r^2) \quad (2.1.9)$$

$$E_{nl\sigma} = \hbar\Omega(2n + l + 1) - \hbar\omega_B l + \sigma E_B, \quad (2.1.10)$$

In equations (2.1.9) and (2.1.10) $n=0,1,2,\dots$, $l = 0, \pm 1, \pm 2, \pm 3, \dots$ are quantum numbers.

Substituting (2.1.8) into $H_e |\psi_I\rangle = \varepsilon_I |\psi_I\rangle$, in principle, we can determine $C_{nl\sigma}^I$, the eigenenergy ε_I , and eigenfunctions, $|\psi_I\rangle = \sum_{nl\sigma} C_{nl\sigma}^I |\mathbf{n} \ l \ \sigma\rangle$, of the total electron system H_e can be obtained.

In order to obtain the expansion coefficients $C_{nl\sigma}^I$, the Hamiltonian is expressed in the form of matrix, and the suitable transformation will be used to make the problem as a finite matrix equation. The matrix form of the Schrödinger equation $H|a\rangle = E|a\rangle$ describing the interacting system may be written as

$$\begin{pmatrix} H_{11} & \dots & H_{1n} \\ \vdots & \ddots & \vdots \\ H_{n1} & \dots & H_{nn} \end{pmatrix} \begin{pmatrix} a_1 \\ \vdots \\ a_n \end{pmatrix} = E \begin{pmatrix} a_1 \\ \vdots \\ a_n \end{pmatrix} \quad (2.1.12)$$

In Eq(2.2.12), the matrix elements are $H_{mn} = \langle m | H | n \rangle$

The matrix equation (2.2.12) may be rewritten

$$\sum_{n=1}^N [H_{mn} - E\delta_{mn}] a_n = 0, \quad m=1,2,\dots,N \quad (2.1.13)$$

which has a nontrivial solution if the characteristic determinant vanishes. The secular equation becomes

$$\begin{vmatrix} H_{11} - E & H_{12} & \dots \\ H_{21} & H_{22} - E & \dots \\ \vdots & \vdots & \ddots \\ \vdots & & & H_m - E \end{vmatrix} = 0$$

For example, consider 12 states are involved in the expansion of (2.1.8).i.e

$$|\psi_L\rangle = \sum_{nl\sigma} C_{nl\sigma} |n l \sigma\rangle = C_1|1\rangle + C_2|2\rangle + C_3|3\rangle + C_4|4\rangle + C_5|5\rangle + C_6|6\rangle + \dots + C_{12}|12\rangle \quad (2.1.14)$$

Substitute into the Schrodinger eq.

$$H_e |\psi_L\rangle = \varepsilon_l |\psi_L\rangle \quad (2.1.15)$$

$$\varepsilon_l |\psi_L\rangle = (H_o + H_{so}) |\psi_L\rangle = \sum_{nl\sigma} C_{nl\sigma} \varepsilon_l |n l \sigma\rangle$$

$$\Rightarrow \langle n' l' \sigma' |$$

$$\sum_{nl\sigma} C_{nl\sigma} E_{nl\sigma} \delta_{nl\sigma}^{n'l'\sigma'} + \sum_{nl\sigma} C_{nl\sigma} \langle n' l' \sigma' | H_{so} | n l \sigma \rangle = \varepsilon_l C_{nl\sigma} \delta_{nl\sigma}^{n'l'\sigma'} \quad (2.1.16)$$

,OR

$$\begin{pmatrix} E_1 + \langle 1|H_{so}|1\rangle & \langle 1|H_{so}|2\rangle & \langle 1|H_{so}|3\rangle & \langle 1|H_{so}|4\rangle & \langle 1|H_{so}|5\rangle & \langle 1|H_{so}|6\rangle \dots \\ \langle 2|H_{so}|1\rangle & E_2 + \langle 2|H_{so}|2\rangle & \langle 2|H_{so}|3\rangle & \langle 2|H_{so}|4\rangle & \langle 2|H_{so}|5\rangle & \langle 2|H_{so}|6\rangle \\ \langle 3|H_{so}|1\rangle & \langle 3|H_{so}|2\rangle & E_3 + \langle 3|H_{so}|3\rangle & \langle 3|H_{so}|4\rangle & \langle 3|H_{so}|5\rangle & \langle 3|H_{so}|6\rangle \\ \langle 4|H_{so}|1\rangle & \langle 4|H_{so}|2\rangle & \langle 4|H_{so}|3\rangle & E_4 + \langle 4|H_{so}|4\rangle & \langle 4|H_{so}|5\rangle & \langle 4|H_{so}|6\rangle \\ \langle 5|H_{so}|1\rangle & \langle 5|H_{so}|2\rangle & \langle 5|H_{so}|3\rangle & \langle 5|H_{so}|4\rangle & E_5 + \langle 5|H_{so}|5\rangle & \langle 5|H_{so}|6\rangle \\ \langle 6|H_{so}|1\rangle & \langle 6|H_{so}|2\rangle & \langle 6|H_{so}|3\rangle & \langle 6|H_{so}|4\rangle & \langle 6|H_{so}|5\rangle & E_6 + \langle 6|H_{so}|6\rangle \dots \end{pmatrix} \begin{pmatrix} C_{00\uparrow} \\ C_{00\downarrow} \\ C_{01\uparrow} \\ C_{01\downarrow} \\ C_{0-1\uparrow} \\ C_{0-1\downarrow} \end{pmatrix} = \varepsilon_l \begin{pmatrix} C_{00\uparrow} \\ C_{00\downarrow} \\ C_{01\uparrow} \\ C_{01\downarrow} \\ C_{0-1\uparrow} \\ C_{0-1\downarrow} \end{pmatrix}$$

In cylindrical coordinates, when the dot lateral size (r) is sufficiently larger than

the dot height (z_0), H_{so} and its matrix elements can be expressed as

$$H_{so}(r, \theta) = \alpha \left\{ -i \left(\frac{\partial}{\partial \rho} \cos \phi + \frac{\partial}{\partial \phi} \left(\frac{-\sin \phi}{\rho} \right) \right) \sigma_x + i \left(\frac{\partial}{\partial \rho} \sin \phi + \frac{\partial}{\partial \phi} \left(\frac{1}{\rho} \cos \phi \right) \right) \sigma_y \right\} \quad (2.1.16)$$

$$\langle n, l, \sigma | H_{so} | n', l', \sigma' \rangle = i2\pi\gamma_c \alpha \delta_{l'+\sigma} \delta_{\sigma, -\sigma'} [\sigma \times D_{n, n', l, l'}^1 - \sigma l' D_{n, n', l, l'}^2 + D_{n, n', l, l'}^3] \quad (2.1.17)$$

The originally spin-conserving electron-phonon scattering has been used in deriving Eq.(2.1.7) to cause spin relaxation. $D_{n, n', l, l'}^1$ to $D_{n, n', l, l'}^3$ in Eq.(2.1.17) are given in detail in the section of results and discussion.

Practical calculation $|\psi_I\rangle$ is expanded in terms of some lowest-energy levels of H_o i.e $|0, 0, \uparrow\rangle, |0, 0, \downarrow\rangle, |0, 1, \uparrow\rangle, |0, 1, \downarrow\rangle, |0, -1, \uparrow\rangle, |0, -1, \downarrow\rangle + \dots$ as basis functions in the perturbation method.

For the spin-orbit coupling H_{so} , mixing occurs for opposite spins:

$$\begin{aligned} \langle n, l, \sigma | H_{so} | n', l', \sigma' \rangle &= \langle n, l | H_{so} | n', l' \rangle \delta_{\sigma, -\sigma'} \\ &= i2\pi\gamma_c \alpha \delta_{l'+\sigma} \delta_{\sigma, -\sigma'} [\sigma \times D_{n, n', l, l'}^1 - \sigma l' D_{n, n', l, l'}^2 + D_{n, n', l, l'}^3] \end{aligned} \quad (2.1.18)$$

After substituting the Pauli matrix, eq.(2.1.5) in cylindrical coordinate can be expanded as :

$$H_{so}(\rho, \phi) = \alpha \left\{ \begin{pmatrix} 0 & ie^{i\phi} \\ -ie^{-i\phi} & 0 \end{pmatrix} \left(-i \left(\frac{1}{\rho} \right) \frac{\partial}{\partial \phi} + \frac{e}{2\hbar} B\rho \right) + \begin{pmatrix} 0 & e^{i\phi} \\ e^{-i\phi} & 0 \end{pmatrix} \left(-i \frac{\partial}{\partial \rho} \right) \right\} \quad (2.1.19)$$

Therefore,

$$\langle n, l | H_{so} | n', l' \rangle \delta_{\sigma, -\sigma'} = \alpha \langle n, l | \left[-i \exp(-i\phi) \left(-i \left(\frac{1}{\rho} \right) \frac{\partial}{\partial \phi} + \frac{e}{2\hbar} B\rho \right) + \exp(-i\phi) \left(-i \frac{\partial}{\partial \rho} \right) \right] | n', l' \rangle \quad (2.1.20)$$

After integration over the angular part, we get the relation $|l - l'| = 1$.

We have three terms:

$$D_{n,n',l,l'}^1 \propto \int_0^\infty \int_0^{2\pi} e^{-\alpha^2 r^2} L_n^l(\alpha^2 r^2) e^{il\phi} (ie^{i\phi}) \frac{e}{\hbar} \mathbf{B} \cdot \mathbf{r} (L_{n'}^{l'}(\alpha^2 r^2) e^{il'\phi}) r dr d\phi \quad (2.1.21)$$

$$D_{n,n',l,l'}^2 \propto \int_0^\infty \int_0^{2\pi} e^{-\alpha^2 r^2} L_n^l(\alpha^2 r^2) e^{il\phi} (ie^{i\phi}) - i \frac{1}{\rho} \frac{\partial}{\partial \phi} (L_{n'}^{l'}(\alpha^2 r^2) e^{il'\phi}) r dr d\phi \quad (2.1.22)$$

$$D_{n,n',l,l'}^3 \propto \int_0^\infty \int_0^{2\pi} (e^{-\alpha^2 r^2} L_n^l(\alpha^2 r^2) e^{il\phi} (ie^{i\phi})) (-i \frac{\partial}{\partial r}) (L_{n'}^{l'}(\alpha^2 r^2) e^{il'\phi}) r dr d\phi \quad (2.1.23)$$

12 states

$|0,0,\uparrow\rangle, |0,0,\downarrow\rangle, |0,1,\uparrow\rangle, |0,1,\downarrow\rangle, |0,-1,\uparrow\rangle, |0,-1,\downarrow\rangle, \dots, |1,-1,\downarrow\rangle$ as basis

functions are used in the perturbation method. The wave function of the lowest two states of H_e are given by

$$\Psi_\uparrow = \langle r | 0,0,\uparrow \rangle - i\hbar\alpha\gamma_c \frac{1 + \frac{eB}{2\hbar\alpha^2}}{E_{0,-1,\uparrow} - E_{0,0,\downarrow}} \langle r | 0,0,\downarrow \rangle \quad (2.1.24)$$

$$\Psi_\downarrow = \langle r | 0,0,\downarrow \rangle - i\hbar\alpha\gamma_c \frac{1 + \frac{eB}{2\hbar\alpha^2}}{E_{0,1,\uparrow} - E_{0,0,\downarrow}} \langle r | 0,0,\uparrow \rangle \quad (2.1.25)$$

$$\Delta E = 2E_B + \left| i\hbar\alpha\gamma_c \frac{1 + \frac{eB}{2\hbar\alpha^2}}{E_{0,1,\uparrow} - E_{0,0,\downarrow}} \right|^2 (E_{0,1,\uparrow} - E_{0,0,\downarrow}) - \left| i\hbar\alpha\gamma_c \frac{1 + \frac{eB}{2\hbar\alpha^2}}{E_{0,-1,\uparrow} - E_{0,0,\downarrow}} \right|^2 (E_{0,-1,\uparrow} - E_{0,0,\uparrow}) \quad (2.1.26)$$

2.2 acoustic phonon

The elasticity equation can be written as (shown as Appendix B)

$$\frac{\partial^2 \mathbf{u}}{\partial t^2} = s_t^2 \nabla^2 \mathbf{u} + (s_l^2 - s_t^2) \nabla(\nabla \cdot \mathbf{u}) \quad (2.2.1)$$

, where \mathbf{u} is the displacement vector, and s_l and s_t are the speeds of longitudinal and transverse acoustic waves. For GaAs, $s_l = 4.78 \times 10^5$ cm/s and $s_t = 3.35 \times 10^5$ cm/s

in the [001] direction. We assume that the width of the wire (rectangular rod) is $2d$ and the thickness of the wire is $2a$, as shown in Figure 1. The acoustic mode with rectangular rod have been examined experimentally (Morse, 1948) and theoretically

(Morse, 1949, 1950). The normal components of the stress tensors must vanish, the boundary conditions for quantum wires are $T_{xx} = T_{yx} = T_{zx} = 0$ at $x = \pm a$, and $T_{xy} = T_{yy} = T_{zy} = 0$ at $y = \pm d$.

In our work, the eigenmodes for acoustic vibrations defined by Eq.(2.2.1) is first obtained. By following Morse's(1950) assumption of separation of variable, the elasticity equation is decomposed by assuming the modes being decomposed into thickness modes and width modes. The solutions can be expressed in the form:

For thickness modes, the displacements are

$$u_x^t = A_t u_t(\gamma, x) \cos(hy) e^{i\gamma(z-ct)} \quad (2.2.2)$$

$$u_y^t = A_t v_t(\gamma, x) \sin(hy) e^{i\gamma(z-ct)} \quad (2.2.3)$$

$$u_z^t = A_t v_t(\gamma, x) \cos(hy) e^{i\gamma(z-ct)} \quad (2.2.4)$$

For width modes, the displacements are

$$u_x^w = A_t u_t(\gamma, y) \sin(hy) e^{i\gamma(z-ct)} \quad (2.2.5)$$

$$u_y^w = A_t v_t(\gamma, y) \cos(hy) e^{i\gamma(z-ct)} \quad (2.2.6)$$

$$u_z^w = A_t v_t(\gamma, z) \cos(hy) e^{i\gamma(z-ct)} \quad (2.2.7)$$

, where γ is the z-directed longitudinal-phonon wave vector along the length of the wire.

To complete the solutions(the dispersion relation for acoustic phonon), we need to find $u_t(\gamma, x), u_w(\gamma, y), v_t(\gamma, y), v_w(\gamma, y), w_t(\gamma, x), w_w(\gamma, y)$. They are found from

the secular equations

$$D_t \begin{pmatrix} u_t(\gamma, x) \\ v_t(\gamma, y) \\ w_t(\gamma, x) \end{pmatrix} = -\omega_n^2 \begin{pmatrix} u_t(\gamma, x) \\ v_t(\gamma, y) \\ w_t(\gamma, x) \end{pmatrix} \quad (2.2.8)$$

, and
$$D_w \begin{pmatrix} v_w(\gamma, y) \\ v_w(\gamma, y) \end{pmatrix} = -\omega_n^2 \begin{pmatrix} v_w(\gamma, y) \\ v_w(\gamma, y) \end{pmatrix} \quad (2.2.9)$$

for thickness and width modes, Eq.(2.2.8),(2.2.9) respectively. Here ω_n is the frequency of the n-th phonon branch for phonon longitudinal wave vector γ . The

matrix operators (thickness D_t and width D_w) are given by

$$D_t = \begin{pmatrix} s_L^2 \frac{\partial^2}{\partial x^2} - s_t^2 (h^2 + \gamma^2) & h(s_L^2 - s_t^2) \frac{\partial}{\partial x} & i\gamma(s_L^2 - s_t^2) \frac{\partial}{\partial x} \\ -h(s_L^2 - s_t^2) \frac{\partial}{\partial x} & s_t^2 \frac{\partial^2}{\partial x^2} - s_t^2 \gamma^2 - s_L^2 h^2 & -i\gamma h(s_L^2 - s_t^2) \\ i\gamma(s_L^2 - s_t^2) \frac{\partial}{\partial x} & i\gamma h(s_L^2 - s_t^2) & s_L^2 \frac{\partial^2}{\partial x^2} - s_t^2 h^2 - s_t^2 \gamma^2 \end{pmatrix} \quad (2.2.10)$$

, and

$$D_w = \begin{pmatrix} s_L^2 \partial_{yy} - s_t^2 \gamma^2 & i\gamma(s_L^2 - s_t^2) \partial_y \\ i\gamma(s_L^2 - s_t^2) \partial_y & s_t^2 \partial_{yy} - s_t^2 \gamma^2 \end{pmatrix} \quad (2.2.11)$$

We solve the one-dimensional eigenvalue problems (2.2.8) and (2.2.9), and use the numerical finite difference scheme. The approximate separation-of-variables solution given by Morse is used for the compressional wave (thickness) modes in the case where $h=h_1=h_2$ and the dilatational wave (width) modes in the case where $q=q_1=q_2$. The dispersion relations for (thickness mode) are :

$$u = (A \sin q_1 x + B \sin q_2 x) \cdot \cos(hy), \quad (2.2.12)$$

$$v = \left(\frac{h}{q_1} A \cos q_1 x + C \cos q_2 x \right) \cdot \sin(hy), \quad (2.2.13)$$

$$w = i \left[\frac{-\gamma}{q_1} A \cos q_1 x + \frac{1}{\gamma} (q_2 B + hC) \cos q_2 x \right] \cos(hy), \quad (2.2.14)$$

$$\text{, where } q_1^2 + h_1^2 = \gamma^2 \left[\left(\frac{c}{c_l} \right)^2 - 1 \right], \quad q_2^2 + h_2^2 = \gamma^2 \left[\left(\frac{c}{c_t} \right)^2 - 1 \right],$$

ρ is the mass density and q_1, q_2 the longitudinal and transverse wave-vector components. They are related to the Lamé' constants λ and μ

$$c_l = \sqrt{\frac{(\lambda + 2u)}{\rho}} \quad (2.2.15)$$

$$c_t = \sqrt{\frac{u}{\rho}} \quad (2.2.16)$$

The boundary conditions for quantum wires are $T_{xx} = T_{yx} = T_{zx} = 0$ at $x = \pm a$.

$$\begin{pmatrix} 2h \sin q_1 a & h \sin q_2 a & q_2 \sin q_2 a \\ -(\gamma^2 + h^2 - q_2^2) \cos q_1 a & 2q_1 q_2 \cos q_2 a & 0 \\ 2(h^2 + \gamma^2) \sin q_1 a & (\gamma^2 + h^2 - q_2^2) \sin q_2 a & 0 \end{pmatrix} \begin{pmatrix} A \\ B \\ C \end{pmatrix} = 0 \quad (2.2.17)$$

The dispersion relation for $q_2 \neq 0$ is given by the expression from the condition that

$$\frac{\tan q_2 a}{\tan q_1 a} = -\frac{4q_1 q_2 (h^2 + \gamma^2)}{(h^2 + \gamma^2 - q_2^2)^2} \quad (2.2.18)$$

We first calculated thickness mode ($h = h_1 = h_2$)

$$\omega_{q\lambda} = c_L \sqrt{\gamma^2 + h^2 + q_1^2} = c_t \sqrt{\gamma^2 + h^2 + q_2^2} \quad (2.2.19)$$

$$\text{, and } \frac{\tan q_2 a}{\tan q_1 a} = -\frac{4q_1 q_2 (h^2 + \gamma^2)}{(h^2 + \gamma^2 - q_2^2)^2} \quad (2.2.20)$$

It is necessary to use a numerical approach to solve Eqs. (2.2.19) and (2.2.20) to find $\omega_{q\lambda}$. However, it is useful to make use of an analytical analysis initially in order to identify different branches and understand their general behavior. The solutions yield the dispersion relations ω_n versus γ . (Figure 12-15). In Figure (12-13), we show the dispersion relations of thickness and width modes for GaAs quantum wire with width = 130nm and thickness = 260nm, and for quantum wire width = 100nm and thickness = 200nm.

2.3 electron-phonon interaction

The interaction between the quantum dot and the acoustic phonon can be expressed as

(shown as 2.3.5)

$$H_{ep} = \sum_q M_q (a_q^\dagger + a_q) e^{iq \cdot r} \quad (2.3.1)$$

The electron-phonon interactions employed in semiconductors have different types of interactions: deformation potential coupling to acoustical phonons, piezoelectric coupling to acoustical phonons, and polar coupling to optical phonons.

The deformation-potential interaction arises from local changes in the crystal's energy bands arising from the lattice distortion created by a phonon.

The deformation-potential interaction, introduced by Bardeen and Shockley, is one of the most important interactions in modern semiconductor devices and it has its origin in the displacements caused by phonons. Thus the phonon displacement field μ produces a local change in the band energy, the energy associated with the change is known as the deformation potential and it represents one of the major scattering mechanics in non-polar semiconductors.

The acoustic phonon in the quantum dot is now considered to interact with the magnetic field. And the deformation-potential (due to strain field) interacting with

acoustic phonon at a certain wave vector γ , can be rewritten in terms of the Hamiltonian H_{e-p} (shown as Eq. (2.3.5) and Eq.(3.315))

$$H_{e-p} = D_a \nabla \cdot u(r), \quad (2.3.2)$$

, where D_a is a deformation-potential coupling constant. The acoustic phonons in rectangular quantum wires composed of rectangular rod (infinite length in the z-direction with an x-directed height $2a$ and a width $2d$ in the y-direction) are shown in Figure 1.

The displacement of acoustic phonon mode is $u(x, y, z) = (u_1, v_1, w_1)$. In the case of quantum wire, the quantization of the acoustic phonons will be performed (as shown in Eq. (3.3.16))

$$u(r) = \sum_{\gamma, n, m} [c_{\alpha\beta}(\gamma) + c_{\alpha\beta}^\dagger(-\gamma)] u(x, y, \gamma) e^{i\gamma z}, \quad (2.3.3)$$

, where $u_1 = u(x, y) e^{i\gamma(z-ct)}$,

$$v_1 = v(x, y) e^{i\gamma(z-ct)},$$

$$w_1 = w(x, y) e^{i\gamma(z-ct)},$$

Substituted Eq.(2.3.3) into Eq.(2.3.2), the deformation potential Eq.(2.3.2) can be rewritten as

$$H_{e-ph} = D_d \sum_{m\gamma} (c_{mn}(\gamma) + c_{mn}^\dagger(-\gamma)) \times \left(\frac{\partial u}{\partial x} + \frac{\partial v}{\partial y} + i\gamma w \right) e^{i\gamma z} \quad (2.3.4)$$

, where $C_{\alpha\beta}$ and $C_{\alpha\beta}^\dagger$ are annihilation and creation operators.

$$\frac{\partial u}{\partial x} = A(k_1 \cos k_1 x + \lambda k_2 \cos k_2 x) \cos(qy) \quad (2.3.5)$$

$$\frac{\partial v}{\partial y} = A\left(\frac{q^2}{k_1} \cos k_1 x + \xi \cos k_2 x\right) \cos(qy) \quad (2.3.6)$$

$$i\gamma w = -A\left(-\frac{\gamma^2}{k_1} \cos k_1 x + (k_2 \lambda + q\xi) \cos k_2 x\right) \cos(qy) \quad (2.3.7)$$

$$\begin{aligned} & \frac{\partial u}{\partial x} + \frac{\partial v}{\partial y} + i\gamma w \\ &= \left(\frac{\omega_\gamma}{c_i^2 k_1}\right) \cos(k_1 x) \cos(hy) + \frac{\omega_\gamma}{2c_i^2 k_2} \left(\frac{h^2}{k_1} \cos k_1 x + h \frac{\sin k_1 a}{\sin k_2 a} \cos k_2 x\right) \cos(hy) \end{aligned} \quad (2.3.8)$$

We estimate the carrier-acoustic phonon rate, it is necessary to evaluate the matrix element of the deformation-potential interaction. The matrix element is given by

$$\begin{aligned} M(E_f', E_i) &= \sum_{n_1, l_1, n_2, l_2, \sigma, -\sigma'} C_{n_1, l_1, \sigma}^i (C_{n_2, l_2, -\sigma'}^f) \left\langle n_2, l_2 \left| \left(\frac{\partial u}{\partial x} + \frac{\partial v}{\partial y} + i\gamma w \right) e^{iyz} \right| n_1, l_1 \right\rangle \\ &= \sum_{n_1, l_1, n_2, l_2, \sigma, -\sigma'} C_{n_1, l_1, \sigma}^i (C_{n_2, l_2, -\sigma'}^{*f}) \left\langle n_2, l_2 \left| \left(\frac{\omega_\gamma}{c_i^2 q_1} \right) \cos(q_1 x) \cos(hy) + \frac{\omega_\gamma}{2c_i^2 q_2} \left(\frac{h^2}{q_1} \cos q_1 x + h \frac{\sin q_1 a}{\sin q_2 a} \cos k_2 x \right) \cos(hy) \right| n_1, l_1 \right\rangle \end{aligned} \quad (2.3.9)$$

An electron is in the initial state $|n_1, l_1\rangle$ with energy $|\varepsilon_i\rangle$ and a spin polarization can be scattered by the phonon into another state $|n_2, l_2\rangle$ with energy $|\varepsilon_f\rangle$ and the opposite spin polarization. For electric-phonon scattering caused by the deformation potential, $|M(E_f, E_i)| = \left| \langle f | H_{e-p} | i \rangle \right|^2$ with $H_{Q\lambda}$ is the matrix for the electron-deformation potential.

Since $M_{Q\lambda}$ will be included in the energy-conserving, and the electron-phonon interacting system is solved by Fermi golden rule. The summation is taken over all acoustic-phonon modes. Spin relaxation rate is from an electron with an energy state E_i to an energy state E_f' by emitting a phonon of wave vector γ and energy

ω_γ is given by (Eq.2.3.9)

The summation is taken over all acoustic-phonon modes.

$$\Gamma_{i \rightarrow f} = \frac{2\pi}{\hbar} \int_{-\infty}^{\infty} d\gamma \left| M(E_f', E_i) \right|^2 \delta(E_f - E_i + \hbar\omega) \quad (2.3.10)$$

, in which

$$\left| M(E_f', E_i) \right|^2 = \left| \sum_{n_1, l_1, n_2, l_2, \sigma, -\sigma'} C_{n_1, l_1, \sigma}^i (C_{n_2, l_2, -\sigma'}^f)^* \left\langle n_2, l_2 \left| \left(\frac{\omega_\gamma}{c_l^2 k_1} \right) \cos(k_1 x) \cos(h y) + \frac{\omega_\gamma}{2c_l^2 k_2} \left(\frac{\hbar^2}{k_1} \cos k_1 x + h \frac{\sin k_1 a}{\sin k_2 a} \cos k_2 x \right) \cos(h y) \right| n_1, l_1 \right\rangle \right|^2 \quad (2.3.11)$$

$$\delta(\varepsilon_f - \varepsilon_i - \omega_{q\lambda}) = \frac{\delta(r - r_1^*)}{|f'(r_1^*)|} + \frac{\delta(r - r_2^*)}{|f'(r_2^*)|} \quad (2.3.12)$$

In the above equation, we change the integration over all possible final states and the energy conservation δ function by summing over all zeros of the function

$$f(r) = \varepsilon_f - \varepsilon_i - \hbar\omega_{q\lambda}$$

$$\omega_{q\lambda} = c_L \sqrt{\gamma^2 + h^2 + k_1^2} = c_i \sqrt{\gamma^2 + h^2 + k_2^2}$$

$$\delta(\varepsilon_f - \varepsilon_i - \omega_{q\lambda}) = \frac{\delta(r - r_1^*)}{|f'(r_1^*)|} + \frac{\delta(r - r_2^*)}{|f'(r_2^*)|} \quad (2.3.13)$$

$$f(r) = 0 \Rightarrow \omega_{q\lambda} = \varepsilon_f - \varepsilon_i = c_L \sqrt{\gamma^2 + h^2 + k_1^2}$$

$$r_1^* = \sqrt{\left(\frac{\varepsilon_f - \varepsilon_i}{c_L} \right)^2 - h^2 - k_1^2}$$

$$r_2^* = \sqrt{\left(\frac{\varepsilon_f - \varepsilon_i}{c_i} \right)^2 - h^2 - k_2^2}$$

$$f'(r) = \frac{-c_L \cdot \gamma - c_L \frac{\partial k_1}{\partial r}}{\sqrt{r^2 + h^2 + k_1^2}}$$

$$f'(r) = \frac{-c_i \cdot \gamma - c_i \frac{\partial k_2}{\partial r}}{\sqrt{r^2 + h^2 + k_2^2}}$$

$$\delta(\varepsilon_f - \varepsilon_i - \omega_{q\lambda}) = \frac{\delta(r - r_1^*)}{\left| \frac{-c_L \cdot \gamma - c_L \frac{\partial k_1}{\partial r_1}}{\sqrt{r_1^2 + h^2 + k_1^2}} \right|} + \frac{\delta(r - r_2^*)}{\left| \frac{-c_i \cdot \gamma - c_i \frac{\partial k_2}{\partial r_2}}{\sqrt{r_2^2 + h^2 + k_2^2}} \right|} \quad (2.3.14)$$

$$\Gamma_{i \rightarrow f} = \frac{2\pi}{\hbar} \int_{-\infty}^{\infty} d\gamma \left| M(E_f', E_i) \right|^2 \delta(E_f - E_i + \hbar\omega) \quad (2.3.15)$$

The spin relaxation time τ can therefore be determined by

$$\frac{1}{\tau} = \sum_i f_i \sum_f \Gamma_{i \rightarrow f} \quad (2.3.16)$$

in which f_i is the Bose-Einstein occupation number $f_i = \frac{1}{\exp(\frac{\varepsilon_i}{kT}) - 1}$ for the acoustic phonon.



Chapter 3

Results and Discussion

Fig.4 shows the electron energy levels in quantum dot without spin-orbit term under a magnetic field. We calculate that $E_{nl\sigma} = \hbar\Omega(2n + l + 1) - \hbar\omega_B l + \sigma E_B$, where $\Omega = \sqrt{\omega_0^2 + \omega_B^2}$, $\omega_B = \frac{eB}{2m^*}$, $E_B = \frac{1}{2} g \mu_B B$. Energy levels for quantum dot with an effective diameter $d=20$ nm and $d=40$ nm, spin orbit coupling is not considered, at least 12-levels $|0,0,\uparrow\rangle$, $|0,0,\downarrow\rangle$, $|0,1,\uparrow\rangle$, $|0,1,\downarrow\rangle$, $|0,-1,\uparrow\rangle$, $|0,-1,\downarrow\rangle$,....., are included. The quantum dot energy level for $d=40$ and $d=20$ ratio is 0.8 with $B < 1$ T.

We calculated $H_e |\psi_l\rangle = \varepsilon_l |\psi_l\rangle$, the eigenenergy ε_l of the total electron system H_e . The calculated spectrum of GaAs quantum dot as a function of the magnetic field B with $n = \pm 1, l = 0, \pm 1$, and $\sigma = \pm 1$. As shown in Figs.5-7 the simulations are presented for the cylindrical quantum dots, for radius of 10nm, 20nm, 40nm, and 60nm, respectively. The GaAs quantum dot is used, thus the effective mass is taken as $0.067 m_0$.

Fig.8 shows the corresponding energy splitting ΔE versus the magnetic field for quantum dot with radius 60nm. We gradually increase the number of basis function when the energy is converged to 0.15% precision. In order to converge the lowest 2

levels, the quantum dot $d=60$ has to use 12 basis functions.

In Fig.9 The crossing levels occur at 0.45T, 0.67T, 1.1T, 1.8T, and 4.02T for quantum dot diameters $d=60\text{nm}$, $d=50\text{nm}$, $d=40\text{nm}$, $d=30\text{nm}$, $d=20\text{nm}$.

The eigenvalue problem of Eqs (2.2.10), (2.2.11), and (2.2.17) can be solved. A major feature of the confined modes is the quantization of the phonon wave in x and y directions. Figs.10-11 show the dispersion relation for the seven lowest different thickness modes and width modes. The thickness mode ($h=h_1=h_2$) is calculated from the following three equations

$$\omega_{q\lambda} = c_L \sqrt{\gamma^2 + h^2 + q_1^2}, \omega_{q\lambda} = c_T \sqrt{\gamma^2 + h^2 + q_2^2}, \quad (3.1.1)$$

and

$$\frac{\tan q_2 a}{\tan q_1 a} = -\frac{4q_1 q_2 (h^2 + \gamma^2)}{(h^2 + \gamma^2 - q_2^2)^2} \quad (3.1.2)$$

There are 4 parameters in this three equations. By keeping $\omega_{q\lambda}$ or γ . One can use a numerical approach to solve the three equations in (2.2.19) and (2.2.20). The dispersion relation for thickness phonon, for a rectangular wire with $130\text{nm} \times 260\text{nm}$, $100\text{nm} \times 200\text{nm}$, respectively. We found the phonon mode with thickness with 1 mode and width with 2 mode as ΔE and phonon coupling numbers. We can calculate the strength of the electric-phonon scattering matrix $M(E_f', E_i)$.

In Fig.12 We present the γ_c which is the spin-orbit coupling strength H_{so} (Dresselhaus coupling)and is the key to understand the spin flip. That is due to

the fact that the spin-orbit coupling H_{so} is proportional $(\frac{1}{a^2})$.

In Fig13, we investigate the magnetic field dependence of the SRT for different radius of the quantum dot at two different temperatures. For larger temperature, the spin relaxation time becomes much larger due to the stronger electron-phonon scattering and the wider range of energy space the electron occupies. The magnetic field dependence of the spin relaxation time for different quantum dot diameter is shown in Fig.13. It is seen that the SRT decreases rapidly with the magnetic field at each dot size. This is because the magnetic field helps to increase the spin-flip. From the Figure, it can be understood that for largest dot, more energy levels are involved in the spin-flip scattering and hence sharply reduce the SRT.



Fig.14 shows the spin relaxation rate gets larger with the increase of the temperature. Moreover, the increase of the temperature comes the phonon number $\bar{n}_{q\lambda}$ to become larger. This enhances the electron-phonon scattering and leads to a larger transition probability.

In Fig.15 we find the spin relaxation time is decreased with the magnetic field. This can be understood from the fact that the energy splitting ΔE increases with the applied magnetic field B and energy splitting required to couple with the phonon mode is increased.

In Figs. 16(a)(b) The spin relaxation time (SRT) of electrons due to the spin-orbit

coupling induces spin-flip electron-phonon scattering at low temperature, where the dominant electron-phonon scattering arises from the deformation potential. Smaller wire width corresponds to larger spin-orbit coupling, therefore, yields as smaller SRT. For larger wire width, more subbands are involved and hence increases an opposite tendency of spin flip i.e a shorter SRT with the increase of the wire width and thickness.



Chapter 4

Conclusions

In this work, we obtained the solutions for the spin relaxation time from exact diagonalization of Hamiltonian to explore its dependence on different magnetic field, temperature, quantum dot, and different width and thickness of the quantum wires.

We found that SRT decreases with the applied magnetic field. This can be understood from the fact that the energy splitting ΔE increases with the applied magnetic field B and more the phonon modes are required to be coupled. Therefore, the electron-phonon scattering probability is larger. The SRT decreases rapidly with the magnetic field at each dot size and temperature. We found that the SRT becomes smaller with the increase of the temperature. The features can be understood by noting that the increase of the temperature will make the phonon number $\overline{n_q}$ to be larger. This enhances the electron-phonon scattering and leads to the larger transition probability.

As the quantum dot is confined in quantum wire, it is necessary to study the width dependence of quantum wire of the SRT. Smaller wire width and thickness correspond to larger spin-orbit coupling and therefore smaller SRT. For larger wire width, more

subbands are involved and hence increase an opposite tendency for a shorter SRT with the increase of the wire width and thickness.

We found that the SRT decreases with the magnetic field. SRT decreases with the diameter of the quantum dot, but increases with the width (thickness) of the quantum wire. With high temperature, SRT becomes longer due to the stronger electron-phonon scattering and the wide-range of energy level the electron occupies.



Appendix A

The Hamiltonian of an electron in external magnetic field derived from a vector potential can be written as:

$$H_e = \frac{1}{2m} \left(P + \frac{e}{c} A \right)^2 - \frac{1}{2} m^* \omega_o^2 \rho^2 \quad (\text{A.1.1})$$

To expand the term of $\left(p + \frac{e}{c} A \right)^2$, we found that \hat{P} does not in general commute with the vector potential \vec{A} , which is a function of the coordinates. Therefore, the Hamiltonian can be expressed as

$$H_e = \frac{p^2}{2m^*} + \frac{1}{2} m^* \omega_o^2 \rho^2 + \frac{e}{m^* c} \vec{A} \cdot \vec{p} + \frac{e^2 A^2}{2m^* c^2} \quad (\text{A.1.2})$$

According to the rule

$$\hat{P} \cdot g(r) - g(r) \cdot \hat{P} = -i\hbar \nabla g(r) \quad (\text{A.1.3})$$

of the momentum operator with any function of the coordinates, we get

$$\hat{P} \cdot \vec{A} - \vec{A} \cdot \hat{P} = -i\hbar \nabla \cdot \vec{A} \quad (\text{A.1.4})$$

The term $\hat{P} \cdot \vec{A}$ can be calculated by analogy with

$$\begin{aligned} \hat{P} \cdot \vec{A} |\psi\rangle &= -i\hbar (\nabla \cdot \vec{A}) |\psi\rangle - i\hbar \vec{A} \cdot \nabla |\psi\rangle \\ &= -i\hbar (\nabla \cdot \vec{A}) |\psi\rangle + \vec{A} \cdot \hat{P} |\psi\rangle \end{aligned} \quad (\text{A.1.5})$$

We see that, whenever $\nabla \cdot \vec{A} = 0$ is valid (the Coulomb gauge), $\vec{A} \cdot \hat{P}$ is equal

to $\hat{P} \cdot \bar{A}$, then

$$\begin{aligned} \left(p + \frac{e}{c} A \right)^2 &= p^2 + \frac{e}{c} p \cdot A + \frac{e}{c} A \cdot p + \frac{e^2}{c^2} A^2 \\ &= p^2 + 2 \frac{e}{c} p \cdot A + \frac{e^2}{c^2} A^2 \end{aligned} \quad (\text{A.1.6})$$

From the theory of classical electromagnetism, the vector potential corresponding to a uniform magnetic field may be written as

$$\bar{A} = \frac{1}{2} (\bar{B} \times \bar{r}) \quad (\text{A.1.7})$$

The equation $-i\hbar \frac{\partial}{\partial t} |\psi\rangle = H_e |\psi\rangle$ with the Hamiltonian Eq(A.1.1) is a generalization of equation to the case where a magnetic field is applied. On the other hands, since $\bar{A} = \frac{1}{2} (\bar{B} \times \bar{r})$, we have

$$\bar{A} \cdot \hat{P} = \frac{1}{2} (\bar{B} \times \bar{r}) \cdot \hat{P} = \frac{1}{2} \bar{B} \cdot (\bar{r} \times \hat{P}) = \frac{1}{2} \bar{B} \cdot \bar{L} \quad (\text{A.1.8})$$

Now, a combination of (A.1.5) leads to $\hat{P} \cdot \bar{A} = \bar{A} \cdot \hat{P} = \frac{1}{2} \bar{B} \cdot \bar{L}$, inserted it in the Hamiltonian

$$H = \frac{p^2}{2m^*} + \frac{1}{2} m^* \omega_o^2 \rho^2 + \frac{e}{2m^*c} B \cdot L + \frac{e^2 A^2}{2m^*c^2} \quad (\text{A.1.9})$$

after the relation $(a \times b) \cdot (c \times d) = (a \cdot c)(b \cdot d) - (a \cdot d)(b \cdot c)$ is used, then

$$\frac{e^2 A^2}{2m^*c^2} = \frac{e^2}{8m^*c^2} (B \times \rho)^2 = \frac{e^2}{8m^*c^2} [B \cdot (r \times (B \times \rho))] \quad (\text{A.1.10})$$

For a particle having a spin with intrinsic magnetic moment μ , the quantum

mechanical operator is proportional to the spin operator \hat{s} , and can be written as

$$\hat{\mu} = \mu \hat{s} \quad (\text{A.1.11})$$

The intrinsic magnetic moment of the particle interacts directly with the magnetic field. The correct expression for the Hamiltonian is obtained by including an extra term $\hat{\mu} \cdot B$ corresponding to the energy of the magnetic moment μ in the field B .

Eq. (A.1.7) now becomes

$$H = \frac{p^2}{2m^*} + \frac{1}{2} m^* \omega_o^2 \rho^2 + \frac{e}{2m^* c} B \cdot L + \frac{e^2}{8m^* c^2} B^2 \rho^2 + \frac{e}{2m^* c} S \cdot B \quad (\text{A.1.12})$$

For an electron in a quantum dot with finite confined potential and an external magnetic field along z axis, the time-independent Schrödinger equation of the electron is:

$$\left\{ \frac{p^2}{2m^*} + \frac{1}{2} m^* \omega_o^2 \rho^2 + \frac{e}{2m^* c} B \cdot L + \frac{e^2}{8m^* c^2} B^2 \rho^2 + \frac{e}{2m^* c} S \cdot B \right\} |\psi\rangle = E |\psi\rangle \quad (\text{A.1.13})$$

In cylindrical coordinate, the operators \hat{P} and \hat{P}^2 are:

$$\hat{P} = \frac{\hbar}{i} \left(\frac{\partial}{\partial \rho} \hat{\rho} + \frac{1}{\rho} \frac{\partial}{\partial \varphi} \hat{\varphi} + \frac{\partial}{\partial z} \hat{z} \right), \quad (\text{A.1.14})$$

$$\text{, and} \quad \hat{P}^2 = -\hbar^2 \left(\frac{1}{\rho} \frac{\partial}{\partial \rho} \left(\rho \frac{\partial}{\partial \rho} \right) + \frac{1}{\rho^2} \frac{\partial^2}{\partial \varphi^2} + \frac{\partial^2}{\partial z^2} \right). \quad (\text{A.1.15})$$

so Eq (A.1.7) becomes:

$$-\frac{\hbar^2}{2m} \left[\frac{1}{\rho} \frac{\partial}{\partial \rho} (\rho \frac{\partial}{\partial \rho}) + \frac{1}{\rho^2} \frac{\partial^2}{\partial \varphi^2} + \frac{\partial^2}{\partial z^2} \right] \psi - \frac{i\hbar}{2} \omega_H \frac{\partial \psi}{\partial \varphi} + \frac{m}{8} \omega_H^2 \rho^2 \psi = E\psi \quad (\text{A.1.16})$$

The equation can be solved by setting

$$|\psi\rangle = |nl\sigma\rangle = R(\rho) \cdot \Phi(\varphi) \cdot \xi(z) \cdot \chi_\sigma \quad (\text{A.1.17})$$

, where $R, \Phi, \xi, \chi_\sigma$ are functions to be determined. For the boundary conditions

$\xi(d) = \xi(-d) = 0$, we can obtain

$$\xi(z) = A \cos\left(\frac{n\pi}{2d} z\right) = A \cos(k \cdot z) \quad (\text{A.1.18})$$

And, for φ component, the single value condition of the wave function $\Phi(\varphi)$ requires:

$$\Phi(\varphi) = e^{il\varphi} \quad l = 0, \pm 1, \pm 2, \pm 3, \dots \quad (\text{A.1.19})$$

we obtain Eq.(A.1.11)

$$\frac{\hbar^2}{2m} \left[\frac{1}{\rho} \frac{\partial}{\partial \rho} (\rho \frac{\partial}{\partial \rho}) - \frac{l^2}{\rho^2} \right] \psi + \left[\frac{\hbar^2 k^2}{2m} + \frac{\hbar}{2} \omega_H + \frac{m}{8} \omega_H^2 \rho^2 - \mu_s \cdot \mathbf{B} \right] \psi = E\psi \quad (\text{A.1.20})$$

Dividing Eq(A.1.17) by $\Phi(\varphi) \cdot \xi(z)$, multiplying it by $\frac{-2m}{\hbar^2}$, and setting

$\varepsilon = E - \frac{\hbar^2 k^2}{2m}$, we get

$$\frac{d^2}{d\rho^2} \phi(\rho) + \frac{1}{\rho} \frac{d}{d\rho} \phi(\rho) + \frac{2m}{\hbar^2} \left[\varepsilon - \frac{\hbar^2 l^2}{2m\rho^2} - \frac{\hbar}{2} \omega_H - \frac{m}{8} \omega_H^2 \rho^2 \right] \phi(\rho) = 0 \quad (\text{A.1.21})$$

, where $\phi(\rho)$ represents the radial part of the electron wave function inside the quantum dot.

We obtain eigenenergy for the quantum dot

$$E_{nl\sigma} = \hbar\Omega(2n + l + 1) - \hbar\omega_B l + \sigma E_B \quad (\text{A.1.22})$$

, where $\Omega = \sqrt{\omega_0^2 + \omega_B^2}$, $\omega_B = \frac{eB}{2m^*}$, $E_B = \frac{1}{2} g \mu_B B$

Define the magnetic length, $l_B = \sqrt{\frac{\hbar c}{eB}}$, and substitute $x = \frac{\rho^2}{2l_B^2}$ into (A.1.22) the term

becomes

$$\frac{\rho^2}{l_B^4} \frac{d^2}{dx^2} \phi(x) + \frac{2}{l_B^2} \frac{d}{dx} \phi(x) + \frac{2m}{\hbar^2} \left[\varepsilon - \frac{\hbar^2 l^2}{2m\rho^2} - \frac{\hbar}{2} \omega_H - \frac{m}{8} \omega_H^2 \rho^2 \right] \phi(x) = 0 \quad (\text{A.1.23})$$

Multiplying Eq. (A.1.20) by $\frac{l_B^2}{2}$, we get

$$\frac{\rho^2}{2l_B^2} \frac{d^2}{dx^2} \phi(x) + \frac{d}{dx} \phi(x) + \frac{ml_B^2}{\hbar^2} \left[\varepsilon - \frac{\hbar^2 l^2}{2m\rho^2} - \frac{\hbar}{2} \omega_H - \frac{m}{8} \omega_H^2 \rho^2 \right] \phi(x) = 0 \quad (\text{A.1.24})$$

Then the equation above can be written as

$$x \frac{d^2}{dx^2} \phi(x) + \frac{d}{dx} \phi(x) + \left[-\frac{x}{4} - \frac{\varepsilon}{2m\rho^2} - \frac{\hbar}{2} \omega_H - \frac{m}{8} \omega_H^2 \rho^2 \right] \phi(x) = 0 \quad (\text{A.1.25})$$

Now, it is necessary to examine the behaviors of the solution $\phi(x)$ of Eq.

(A.1.22) at the origin and infinity in order to know if they are well behaved. We

require the wave function to be finite everywhere. Dividing Eq. (A.2.22) by x, we get

$$\frac{d^2}{dx^2} \phi(x) + \frac{1}{x} \frac{d}{dx} \phi(x) + \left[-\frac{1}{4} + \frac{1}{x} \left(\frac{\varepsilon}{\hbar\omega_H} - \frac{l}{2} \right) - \frac{l^2}{4x^2} \right] \phi(x) = 0 \quad (\text{A.1.26})$$

(I) when x approaches zero, Eq.(A.2.23) can be reduced to

$$\frac{d^2}{dx^2} \phi(x) + \frac{1}{x} \frac{d}{dx} \phi(x) - \frac{l^2}{4x^2} \phi(x) = 0 \quad (\text{A.1.27})$$

By setting $\phi(x) = x^r \sum_{n=0}^{\infty} a_n x^n$ (A.1.28)

And substituting Eq. (A.1.25) into Eq. (A.1.24), we get

$$\sum_{n=0}^{\infty} \left[(n+r)(n+r-1)a_n x^{n+r-2} + (n+r)a_n x^{n+r-2} - \frac{l^2}{4} a_n x^{n+r-2} \right] = 0 \quad (\text{A.1.29})$$

The coefficients of polynomials should equal to zero to satisfy Eq. (A.1.25), that is,

$$(n+r)(n+r-1) + (n+r) - \frac{l^2}{4} = 0 \quad (\text{A.1.30})$$

Finally, we get $n+r = \pm \frac{l}{2}$. So that, x^{n+r} equal to $x^{\frac{|l|}{2}}$ or $x^{-\frac{|l|}{2}}$. Here

$l = 0, \pm 1, \pm 2, \pm 3, \dots$. Since $x^{-\frac{|l|}{2}}$ diverges as x approaches zero, $\phi(x) \sim x^{\frac{|l|}{2}}$ is chosen for the case as x approaches zero.

(II) As x approaches infinity, Eq.(A.1.23) can be written as

$$\frac{d^2}{dx^2} \phi(x) - \frac{1}{4x^2} \phi(x) = 0 \quad (\text{A.1.31})$$

Setting $\phi(x) = e^{mx}$ and substituting it into Eq. (A.1.23), we can obtain the

relations: $m^2 - \frac{1}{4} = 0$ (A.1.32)

So, we get $m = \pm \frac{1}{2}$, and $\phi(x) \sim e^{-x/2}$ or $\phi(x) \sim e^{x/2}$. As x approaches infinity, $e^{x/2}$

will diverge, so we choose $\phi(x) \sim e^{-x/2}$ as x approached infinity.

Now we may set the solution of Eq. (A.1.24) to be

$$\phi(x) = e^{-x/2} \cdot x^{\frac{|l|}{2}} \cdot X(x) \quad (\text{A.1.33})$$

Substituting Eq. (A.1.24) into Eq. (A.1.25) and simplifying the resulted equation, we

get

$$x \frac{d^2}{dx^2} X + [|l| + 1 - x] \frac{d}{dx} X + \left[\frac{\varepsilon}{\hbar \omega_H} - \frac{l + |l| + 1}{2} \right] X = 0 \quad (\text{A.1.34})$$

We compare the equation with the confluent hypergeometric function:

$$\beta \frac{d^2}{d\beta^2} F + [\chi - \beta] \frac{d}{d\beta} F - \lambda F = 0 \quad (\text{A.1.35})$$

, where $F = {}_1F_1(\lambda, \chi, \beta)$ is the confluent hypergeometric function. The solution of

$X(x)$ is satisfied by the confluent hypergeometric function, we have

$$\begin{aligned} X(x) &= F_1 \left(- \left[\frac{\varepsilon}{\hbar \omega_H} - \frac{l + |l| + 1}{2} \right], |l| + 1, x \right) \\ &= {}_1F_1(\lambda, |l| + 1, x) \end{aligned} \quad (\text{A.1.36})$$

, where

$$\lambda = - \left[\frac{\varepsilon}{\hbar \omega_H} - \frac{l + |l| + 1}{2} \right] \quad (\text{A.1.37})$$

, and may be determined by the boundary condition.

Therefore we obtain

$$\psi = A \cdot e^{-x/2} \cdot x^{|l|/2} \cdot {}_1F_1(\lambda, |l| + 1, x) \cdot e^{il\varphi} \cdot \cos\left(\frac{n\pi}{2d} z\right) \quad (\text{A.1.38})$$

where A is the normalized constant. Eq.(A.1.22) can be rewritten as

$$\psi(\rho, \varphi, z) = A e^{-m\omega_H \rho^2 / 4\hbar} \cdot \left(\frac{m\omega_H}{2\hbar} \rho^2 \right)^{|l|/2} \cdot {}_1F_1\left(\lambda, |l| + 1, \frac{m\omega_H}{2\hbar} \rho^2\right) \cdot e^{il\varphi} \cdot \cos\left(\frac{n\pi}{2d} z\right) \quad (\text{A.1.39})$$

${}_1F_1(a, c, z)$ becomes a polynomial function, when suitably normalized, is a Laguerre

polynomial. Specifically, one usually writes

$$L_n^\alpha(z) = \frac{\Gamma(\alpha + n + 1)}{n!} / \Gamma(\alpha + 1) \cdot {}_1F_1(-n, \alpha + 1, z) \quad (\text{A.1.40})$$

We obtain

$$|nl\sigma\rangle = R_{nl} e^{il\theta} \chi_\sigma = \sqrt{\left[\frac{\alpha^2 n!}{\pi(n + |l|)!} \right]} (\alpha r)^{|l|} \exp\left(-\frac{(\alpha r)^2}{2}\right) L_n^{|l|}(\alpha^2 r^2) \quad (\text{A.1.41})$$



Appendix B

Definition of stress and strain:

The intensity of the force, the force per unit area, is defined to be the stress. Let the components of ΔF along x, y, z axes be $\Delta F_x, \Delta F_y, \Delta F_z$. Stress components are defined as

$$\sigma_x = \lim_{\Delta A \rightarrow 0} \frac{\Delta F_x}{\Delta A} \quad (\text{B.1.1})$$

$$\tau_{xy} = \lim_{\Delta A \rightarrow 0} \frac{\Delta F_y}{\Delta A} \quad (\text{B.1.2})$$

$$\tau_{xz} = \lim_{\Delta A \rightarrow 0} \frac{\Delta F_z}{\Delta A} \quad (\text{B.1.3})$$



, where σ_x is the normal stress and τ_{xy}, τ_{xz} are the shear stresses.

Normal stress is the intensity of a force perpendicular to a cut curve while the shear stress is parallel to the plane of the element.

There are three normal stresses $\sigma_x, \sigma_y, \sigma_z$ where the axis along which is the normal to the cut plane. There are also six shear stresses $\tau_{xy}, \tau_{yx}, \tau_{yz}, \tau_{zy}, \tau_{zx}, \tau_{xz}$, where the first subscript denotes the axis perpendicular to the plane on which the stress acts and the second provides the direction of the stress. For example, the shear stress τ_{yx} acts on a plane normal to the y axis and in a direction parallel to the x axis.

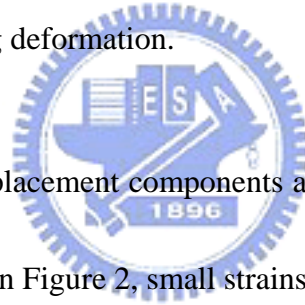
In matrix form, the stress components appear as

$$[\mathbf{T}] = \begin{pmatrix} \sigma_x & \tau_{xy} & \tau_{xz} \\ \tau_{yx} & \sigma_y & \tau_{yz} \\ \tau_{zx} & \tau_{zy} & \sigma_z \end{pmatrix} \quad (\text{B.1.4})$$

The matrix of stress is called a stress tensor.

Definition of strain:

The strain can be defined in terms of normal and shear strains. Normal strain is defined as the change in length per unit length of a line segment in the direction under consideration. Shear strain is defined as the tangent of the change in angle of a right angle in a member undergoing deformation.



If u , v , w are three displacement components at a point in a body for the x , y , z directions of coordinate axes in Figure 2, small strains are related to the displacements through the geometric relationships.

$$S_1 = S_{xx} = \frac{\partial u}{\partial x} \quad (\text{B.1.5})$$

$$S_2 = S_{yy} = \frac{\partial v}{\partial y} \quad (\text{B.1.6})$$

$$S_3 = S_{zz} = \frac{\partial w}{\partial z} \quad (\text{B.1.7})$$

$$S_4 = S_{yz} = S_{zy} = \frac{1}{2} \left(\frac{\partial w}{\partial y} + \frac{\partial v}{\partial z} \right) \quad (\text{B.1.8})$$

$$S_5 = S_{xz} = S_{zx} = \frac{1}{2} \left(\frac{\partial u}{\partial z} + \frac{\partial w}{\partial x} \right) \quad (\text{B.1.9})$$

$$S_6 = S_{xy} = S_{yx} = \frac{1}{2} \left(\frac{\partial u}{\partial y} + \frac{\partial v}{\partial x} \right) \quad (\text{B.1.10})$$

Let $u(x)$ be the elastic displacement at x along the axis of the one-dimensional structure, and $u(x)$ describes the uniform longitudinal displacement of the element dx .

In the elastic model the dynamics of phonon cavity, dx , is described in terms of Newton's laws. It follows from Hooke's law that

$$T = Y \cdot S, \quad (\text{B.1.11})$$

where Y is a Young's modulus. The force equation describing the dynamics of the element dx of density $\rho(x)$ is given by Newton's law;

$$\rho(x)A dx \frac{\partial^2 u(x,t)}{\partial t^2} = [T(x+dx) - T(x)]A, \quad (\text{B.1.12})$$

, where $\rho(x)A dx$ is the mass associated with the index dx and $\frac{\partial^2 u}{\partial t^2}$.

By Hooke's law

$$T(x+dx) - T(x) = \left(\frac{\partial T}{\partial x}\right)dx = \left(Y \frac{\partial S}{\partial x}\right)dx = \left(Y \frac{\partial^2 u}{\partial x^2}\right)dx \quad (\text{B.1.13})$$

and it follows that

$$\frac{\partial^2 u}{\partial x^2} = \left(\frac{\rho(x)}{Y}\right) \frac{\partial^2 u}{\partial t^2} \quad (\text{B.1.14})$$

stress and strains independent of variable.

$$\begin{aligned} T_1 &= T_{xx} \\ T_2 &= T_{yy} \\ T_3 &= T_{zz} \\ T_4 &= T_{yz} = T_{zy} \quad , \text{ the form by six-element.} \\ T_5 &= T_{zx} = T_{xz} \\ T_6 &= T_{xy} = T_{yx} \end{aligned}$$

$$[\mathbf{T}] = \begin{bmatrix} T_1 \\ T_2 \\ T_3 \\ T_4 \\ T_5 \\ T_6 \end{bmatrix}, \quad [\mathbf{S}] = \begin{bmatrix} S_1 \\ S_2 \\ S_3 \\ S_4 \\ S_5 \\ S_6 \end{bmatrix}, \quad [\mathbf{C}] = \begin{pmatrix} C_{11} & C_{12} & C_{13} & C_{14} & C_{15} & C_{16} \\ C_{21} & C_{22} & C_{23} & C_{24} & C_{25} & C_{26} \\ C_{31} & C_{32} & C_{33} & C_{34} & C_{35} & C_{36} \\ C_{41} & C_{42} & C_{43} & C_{44} & C_{45} & C_{46} \\ C_{51} & \dots & \dots & \dots & \dots & \dots \\ C_{61} & \dots & \dots & \dots & \dots & \dots \end{pmatrix} \quad (\text{B.1.15})$$

For the zincblende crystals, the stress-strain relation is the most general form, the matrix C_{ij} is of the form (the zincblende crystal have only three independent elastic constants, C_{11}, C_{12}, C_{44}).

$$\begin{pmatrix} C_{11} & C_{12} & C_{12} & 0 & 0 & 0 \\ C_{12} & C_{11} & C_{23} & 0 & 0 & 0 \\ C_{12} & C_{12} & C_{11} & 0 & 0 & 0 \\ 0 & 0 & 0 & C_{44} & 0 & 0 \\ 0 & 0 & 0 & 0 & C_{44} & 0 \\ 0 & 0 & 0 & 0 & 0 & C_{44} \end{pmatrix} \Rightarrow \begin{pmatrix} \lambda + 2\mu & \lambda & \lambda & 0 & 0 & 0 \\ \lambda & \lambda + 2\mu & \lambda & 0 & 0 & 0 \\ \lambda & \lambda & \lambda & 0 & 0 & 0 \\ 0 & 0 & 0 & \mu & 0 & 0 \\ 0 & 0 & 0 & 0 & \mu & 0 \\ 0 & 0 & 0 & 0 & 0 & \mu \end{pmatrix} \quad (\text{B.1.16})$$

There are two constants λ and μ necessary to define the C_{ij}

$$\text{By } [\mathbf{T}] = [\mathbf{C}][\mathbf{S}] \quad (\text{B.1.17})$$

$$\Rightarrow \begin{cases} T_{xx} = \lambda(S_{xx} + S_{yy} + S_{zz}) + 2\mu S_{xx} \\ T_{yy} = \lambda(S_{xx} + S_{yy} + S_{zz}) + 2\mu S_{yy} \\ T_{zz} = \lambda(S_{xx} + S_{yy} + S_{zz}) + 2\mu S_{zz} \\ T_{yz} = \mu S_{yz} \\ T_{zx} = \mu S_{zx} \\ T_{xy} = \mu S_{xy} \end{cases} \quad (\text{B.1.18})$$

$$\Rightarrow \begin{cases} \text{x director : } \frac{\partial T_1}{\partial x} + \frac{\partial T_6}{\partial y} + \frac{\partial T_5}{\partial z} = \rho \frac{\partial^2 \mu}{\partial t^2} \\ \text{y director : } \frac{\partial T_6}{\partial x} + \frac{\partial T_2}{\partial y} + \frac{\partial T_4}{\partial z} = \rho \frac{\partial^2 v}{\partial t^2} \\ \text{z director : } \frac{\partial T_5}{\partial x} + \frac{\partial T_4}{\partial y} + \frac{\partial T_3}{\partial z} = \rho \frac{\partial^2 w}{\partial t^2} \end{cases}$$

$$\Rightarrow \begin{cases} \text{x director : } \rho \frac{\partial^2 \mu}{\partial t^2} = \frac{\partial T_{xx}}{\partial x} + \frac{\partial T_{yx}}{\partial y} + \frac{\partial T_{zx}}{\partial z} = (\lambda + \mu) \frac{\partial \Delta}{\partial x} + \mu \nabla^2 \mu \\ \text{y director : } \rho \frac{\partial^2 v}{\partial t^2} = \frac{\partial T_{xy}}{\partial x} + \frac{\partial T_{yy}}{\partial y} + \frac{\partial T_{zy}}{\partial z} = (\lambda + \mu) \frac{\partial \Delta}{\partial x} + \mu \nabla^2 \mu \\ \text{z director : } \rho \frac{\partial^2 w}{\partial t^2} = \frac{\partial T_{xz}}{\partial x} + \frac{\partial T_{yz}}{\partial y} + \frac{\partial T_{zz}}{\partial z} = (\lambda + \mu) \frac{\partial \Delta}{\partial x} + \mu \nabla^2 \mu \end{cases} \quad \text{elastic-wave equation}$$

In general:

$$\rho \frac{\partial^2 \mu_\alpha}{\partial t^2} = \frac{\partial T_{\alpha\beta}}{\partial \gamma_\beta}, \quad (\text{B.1.19})$$

where ρ is the density of a semiconductor and $T_{\alpha\beta}$ is the stress tensor.

Then the stress tensor is

$$T_{\alpha\beta} = \lambda S_{\alpha\alpha} \delta_{\alpha\beta} + 2\mu S_{\alpha\beta} \quad (\text{B.1.20})$$

, where λ and μ are elastic moduli, or Lamé' constant, and $\delta_{\alpha\beta}$ is Kronecker delta

For an isotropic medium, Eq.(B.1.19) can be rewritten in vector form as

$$\frac{\partial^2 \boldsymbol{\mu}_\alpha}{\partial t^2} = s_t^2 \nabla^2 \boldsymbol{\mu}_\alpha + (s_t^2 - s_L^2) \text{grad div}(\boldsymbol{\mu}_\alpha) \quad (\text{B.1.21})$$

, where $s_t^2 = \frac{\mu}{\rho}$ and $s_L^2 = \frac{\lambda + 2\mu}{\rho}$

are the velocities of the LA and the TA waves in bulk semiconductors



Appendix C.1

The Hamiltonian describing the harmonic oscillator associated with a phonon mode of wavevector q is

$$H_q = \frac{P_q^2}{2m} + \frac{1}{2}m\omega_q^2\mu_q^2 \quad (\text{C.1.1})$$

, where m is the mass of the oscillator, ω_q is frequency of the phonon, μ_q is the displacement associated with it, and p_q is kinetic momentum.

Introducing the operators, a_q and a_q^+ , and

$$a_q = \sqrt{\frac{m\omega_q}{2\hbar}}\mu_q + i\sqrt{\frac{1}{2\hbar m\omega_q}}p_q \quad (\text{C.1.2})$$

$$a_q^+ = \sqrt{\frac{m\omega_q}{2\hbar}}\mu_q - i\sqrt{\frac{1}{2\hbar m\omega_q}}p_q, \quad (\text{C.1.3})$$

$$a_q^+a_q = \left(\sqrt{\frac{m\omega_q}{2\hbar}}\mu_q - i\sqrt{\frac{1}{2\hbar m\omega_q}}p_q\right)\left(\sqrt{\frac{m\omega_q}{2\hbar}}\mu_q + i\sqrt{\frac{1}{2\hbar m\omega_q}}p_q\right) \quad (\text{C.1.4})$$

Here the commutator $[\mu_q, p_q] = \mu_q p_q - p_q \mu_q = i\hbar$ comes from the properties of the quantum mechanical operators .

Thus phonon energy is:

$$\frac{p_q^2}{2m} + \frac{1}{2}m\omega_q^2\mu_q^2 = \hbar\omega_q\left(a_q^+a_q + \frac{1}{2}\right) \quad (\text{C.1.5})$$

Appendix C.2

It will be convenient to express the normal-mode phonon displacement μ_q in terms of the phonon creation and annihilation operators.

$$\mu_q = \sqrt{\frac{\hbar}{2m\omega_q}}(a_q + a_q^\dagger) \quad (\text{C.2.1})$$

Moreover, each incoming or outgoing phonon will be associated with a unit polarization vector, these unit polarization vectors will be denoted by $\hat{e}_{q,j}$ for incoming waves and by $\hat{e}_{q,j}^*$ for outgoing waves.

$$\begin{aligned} \mu(r) &= \frac{1}{\sqrt{N}} \sum_q \sum_{j=1,2,3} \sqrt{\frac{\hbar}{2m\omega_q}} (a_q e^{iq \cdot r} \hat{e}_{q,j} + a_q^\dagger e^{-iq \cdot r} \hat{e}_{q,j}^*) \\ &= \frac{1}{\sqrt{N}} \sum_q \sum_{j=1,2,3} \sqrt{\frac{\hbar}{2m\omega_q}} \hat{e}_{q,j} (a_q + a_{-q}^\dagger) e^{iq \cdot r} \equiv \sum_q \mu(q) e^{iq \cdot r} \end{aligned} \quad (\text{C.2.2})$$

, where q is summed over all wavevectors in the Brillouin zone and N is the number of unit cells in the sample.

The interaction between the quantum dot and the acoustic phonon can be expressed as

$$H_{ep} = \sum_q M_q (a_q^\dagger + a_q) e^{iq \cdot r} \quad (\text{C.2.3})$$

For long wavelengths we can treat the one-dimensional chain and the strain becomes a derivative.

The longitudinal strain is

$$e(z) = \frac{\partial \mu}{\partial z} = -\sqrt{\frac{2\hbar}{\Omega \rho \omega_q}} q \sin(qz - \omega_q t) \quad (\text{C.2.4})$$

The deformation potential energy can be calculated as through the strain.

$$H_{e-p} = \Xi e(z) = -\sqrt{\frac{2\hbar}{\Omega \rho \omega_q}} q \Xi \sin(qz - \omega_q t) = i \sqrt{\frac{\hbar}{2\Omega \rho \omega_q}} \Xi (e^{iqz} - e^{-iqz}) \quad (\text{C.2.5})$$

This is the form of the perturbing potential caused by the phonon to be used in Fermi's golden rule.

The piezoelectric interaction occurs in all polar crystal lacking an inversion symmetry. In rectangular coordinates, the polarization created by the piezoelectric interaction in cubic crystals, including zincblende crystals, may be written as

$$P = \left\{ \frac{1}{2} e_{x4} \left(\frac{\partial w}{\partial y} + \frac{\partial v}{\partial z} \right), \frac{1}{2} e_{x4} \left(\frac{\partial \mu}{\partial z} + \frac{\partial w}{\partial x} \right), \frac{1}{2} e_{x4} \left(\frac{\partial \mu}{\partial y} + \frac{\partial v}{\partial x} \right) \right\}, \quad (\text{C.2.6})$$

, where e_{x4} is the piezoelectric coupling constant and the factors multiplying e_{x4} are the components of the strain tensor that contribute to the piezoelectric polarization in a zincblende crystal.

References

- [1] O. Voskoboynikov, C. P. Lee, and O. Tretiyak, Phys.Rev.B,63 165306(2001)
- [2] A. Svizhenko, A. Balandin, and S. Bandyopadhyay Michael A. Stroschio, Phys.Rev.B,57 4687(1998)
- [3] A.Einstein, Phys.Z. 18,121(1917)
- [4] Semiconductor Spintronics and Quantum Computation, edited by D.D. Awschalom, D Loss, Springer (2002)
- [5] C. F. Destefani, Sergio E. Ulloa, and G. E. Marques, Phys. Rev. B **69**, 125302 (2004)
- [6] Alexander V. Khaetskii and Yuli V. Nazarov, Phys. Rev. B 64, 125316 (2001)
- [7] Manuel Valín-Rodríguez, Antonio Puente, and Llorenç Serra, Phys. Rev. B **69**, 085306 (2004)
- [8] Manuel Valín-Rodríguez, Antonio Puente, and Llorenç Serra, Phys. Rev. B **66**, 165302 (2002)
- [9] R. Hanson, B. Witkamp, L. M. K. Vandersypen, L. H. Willems van Beveren, J. M. Elzerman, and L. P. Kouwenhoven Phys. Rev. Lett. **91**, 196802 (2003)
- [10] N. Bannov, V. Aristov, and V. Mitin Michael A. Stroschio, Phys.Rev.B 51,9930(1995)
- [11] SeGi Yu and K. W. Kim Michael A. Stroschio, Phys.Rev.B,51 4695(1995)
- [12] T. Brandes, Phys.Rev.B,66 041301(2002)
- [13] J. L. Cheng, M. W. Wu, and C. Lü, Phys.Rev.B,69 115318(2004)
- [14] M. Governale, Phys. Rev. Lett. 89, 206802 (2002)

- [15] Vitaly N. Golovach, Alexander Khaetskii, and Daniel Loss Phys. Rev. Lett. **93**, 016601 (2004)
- [16] W.H.Kuan W.Xu Journal of Applied Phys. **95**,6368
- [17] Y. Ohno, R. Terauchi, T. Adachi, F. Matsukura, and H. Ohno, Phys. Rev. Lett. **83**, 4196 (1999)
- [18]A.M.Alcalde,G.E.Marques, J of Phys 34 No2B (2004)
- [19] J.P.Leburton, J.A.Phys, **56** 15(1984)
- [20] O. Voskoboynikov ,C. P. Lee, and O. Tretyak, Physica E **10** 107 (2001)
- [21] Michael A. Stroscio, Phys.Rev.B,**40** 6428(1989)
- [22] N. Telang and S. Bandyopadhyay, Phys.Rev.B,**48** 18002(1993)
- [23]L. M. Woods, T. L. Reinecke, and Y. Lyanda-Geller, Phys.Rev.B,**66** 161318(2002)
- [24] Alexander V. Khaetskii* and Yuli V. Nazarov, Phys.Rev.B,**61** 12639(2000)
- [25] Rogerio de Sousa and S. Das Sarma Phys. Rev. B **68**, 155330 (2003)
- [26] B. A. Glavin and V. I. Pipa Michael A. Stroscio, Phys.Rev.B,**65** 205315(2002)
- [27] B. K. Ridley, Phys.Rev.B,**39** 5282(1989)
- [28] Michael A. Stroscio,J. Appl. Phys.**70** 1 (1991)
- [29] SeGi Yu and K. W. Kim Michael A. Stroscio, Phys.Rev.B,**50** 1733(1994)
- [30] David M. Frenkel Phys. Rev. B **43**, 14228 (1991)
- [31] E. M. Weig,R. H. Blick, T. Brandes, J. Kirschbaum, W. Wegscheider, M. Bichler, and J. P. Kotthaus,Phys.Rev.L **92** 046804(2004)
- [32]F.Geerinckx, J.A.Phys, **68** 1 (1990)

- [33]J.Bardeen, Phys.Rev.80,1(1950)
- [34]J.M.Elzerman, R. Hanson .Nature.430 22(2004)
- [35]Daniel. Loss,Phys.Rev.B 71 ,205324 (2005)
- [36]Rogerio De Sousa,Phys.Rev.B 68 155330(2003)
- [37]P.Tonello,Phys.Rev.B 70 081201(R) (2004)
- [38]Alexander. Balandin, PRB 58 1544 (1998)
- [39]C.F.Destefani,Phys.Rev.B 71 161303 (2005)
- [40]C.F.Destefani,arXiv:cond-mat/0412520 (2004)



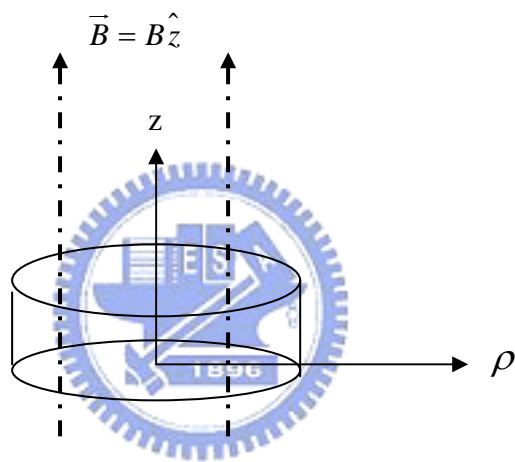


Fig.1 The cylindrical-shaped quantum dot in an applied magnetic field.

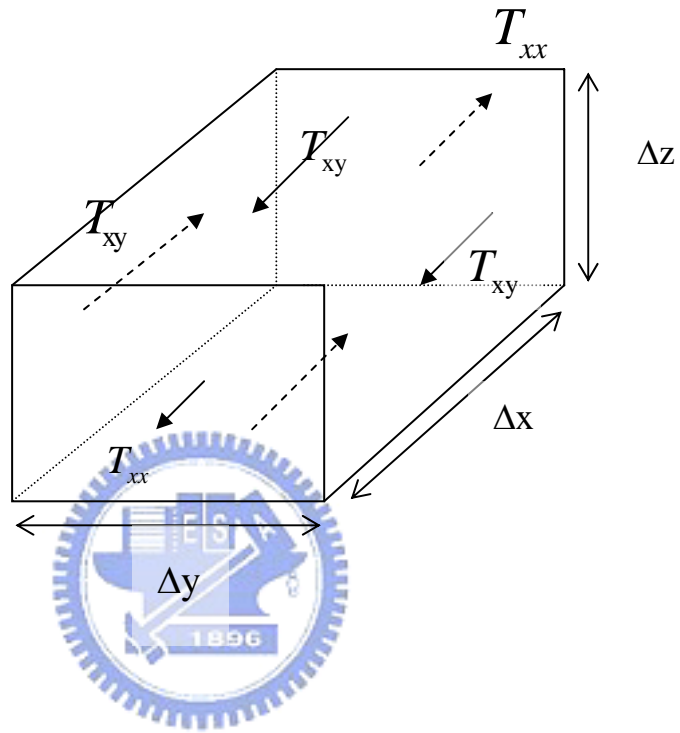


Fig.2 For a cubic medium , volume of cube is $\Delta x \Delta y \Delta z$

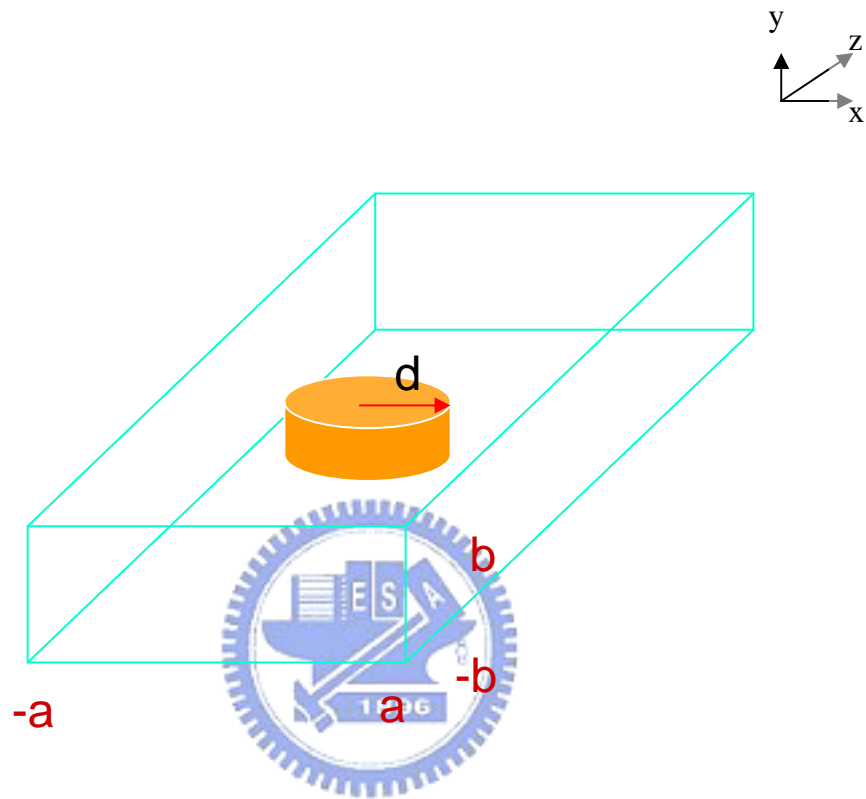


Fig.3 A rectangular rod of infinite length in z-direction with a height $2a$ in x-direction and a width $2d$ in the y-direction.

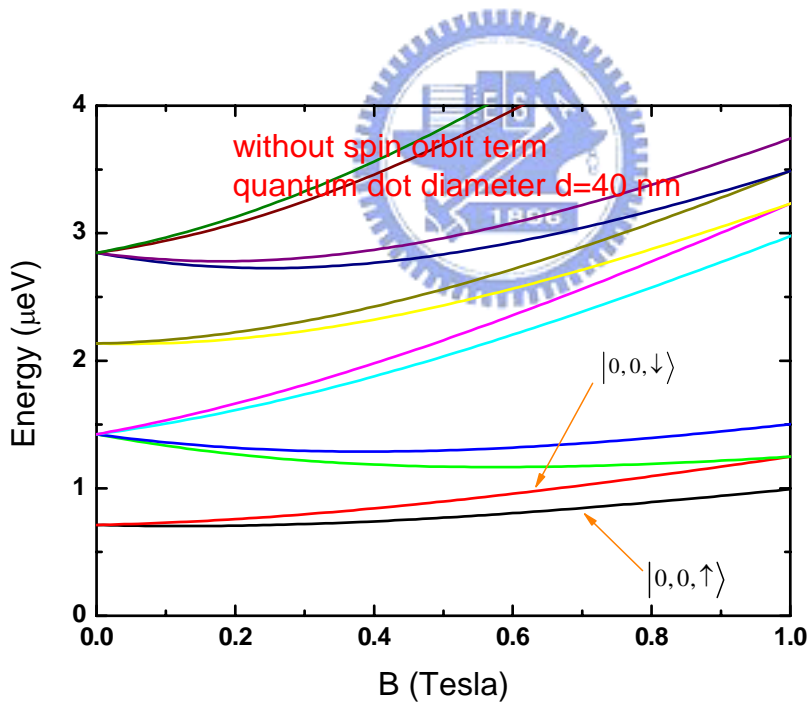
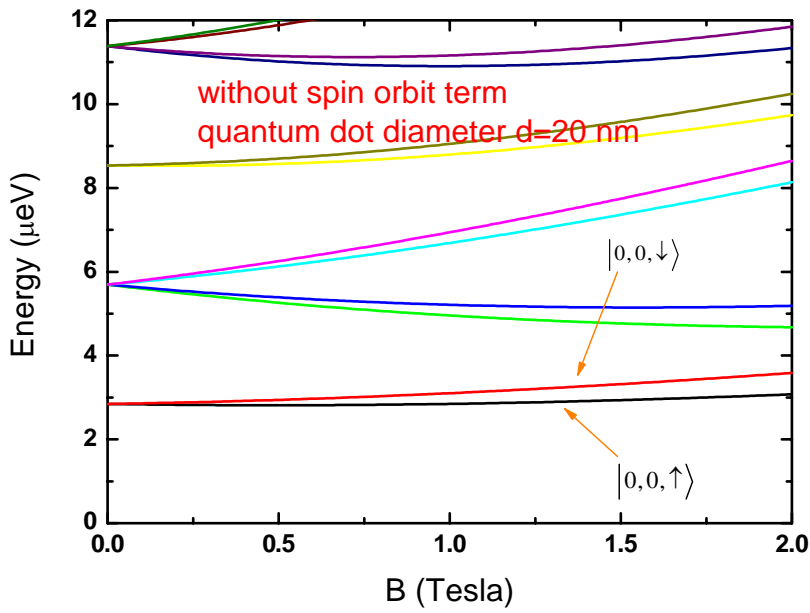


Fig.4 Energy levels for quantum dot with an effective diameter $d=20$ nm and $d=40$ nm , spin orbit coupling is not included , at least 12-levels

$$|0,0,\uparrow\rangle, |0,0,\downarrow\rangle, |0,1,\uparrow\rangle, |0,1,\downarrow\rangle, \dots, |1,1,\downarrow\rangle, |1,-1,\uparrow\rangle, |1,-1,\downarrow\rangle$$

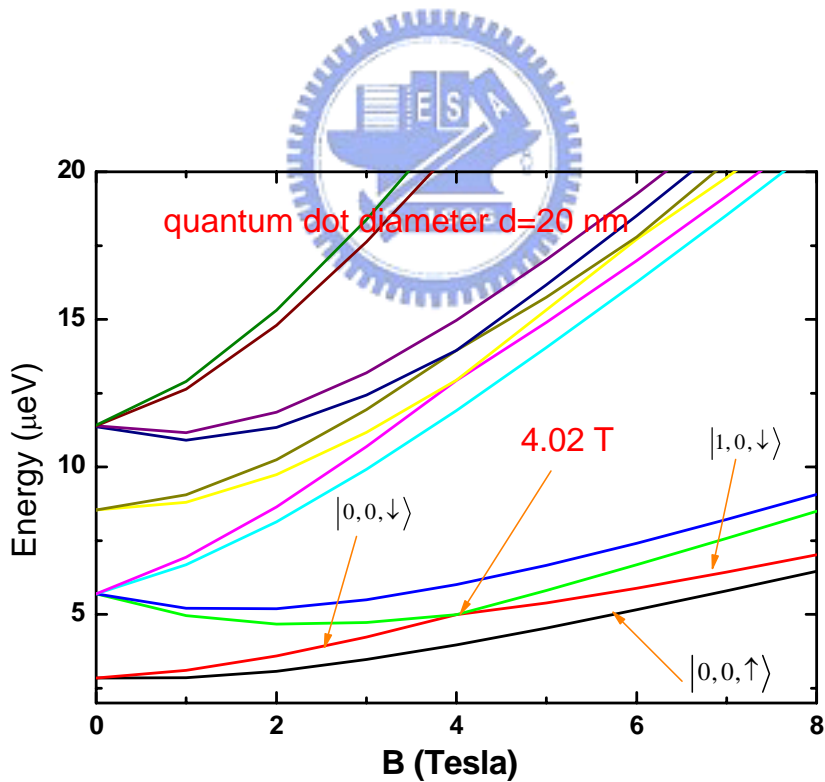
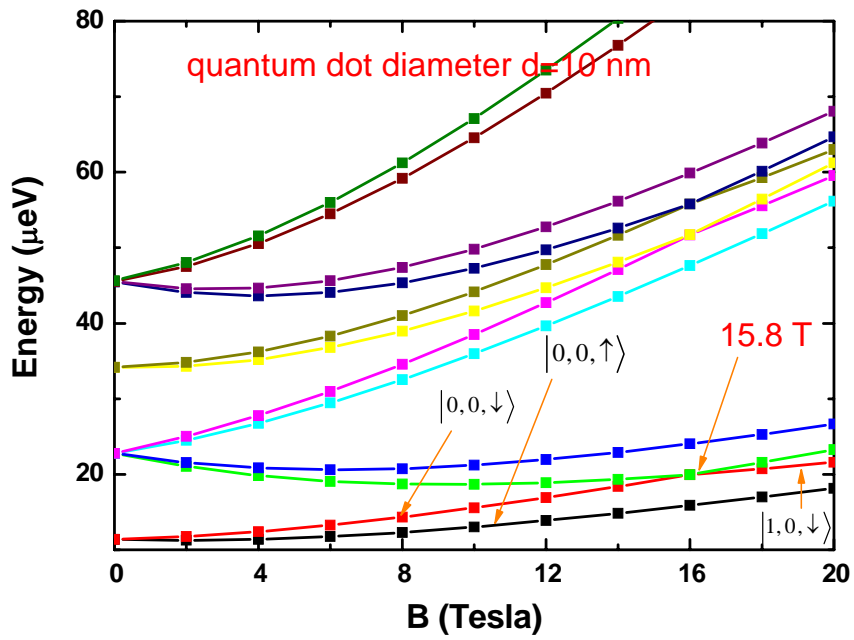


Fig.5 Energy levels for quantum dot with an effective diameter $d=10$ nm, $d=20$ nm, respectively with including Dressshauls effective interaction.

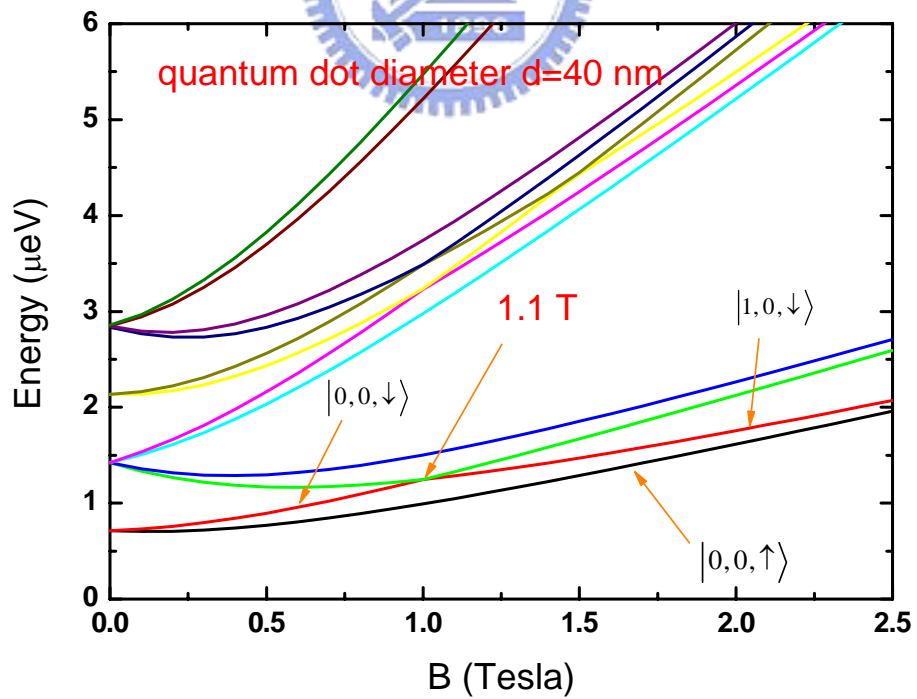
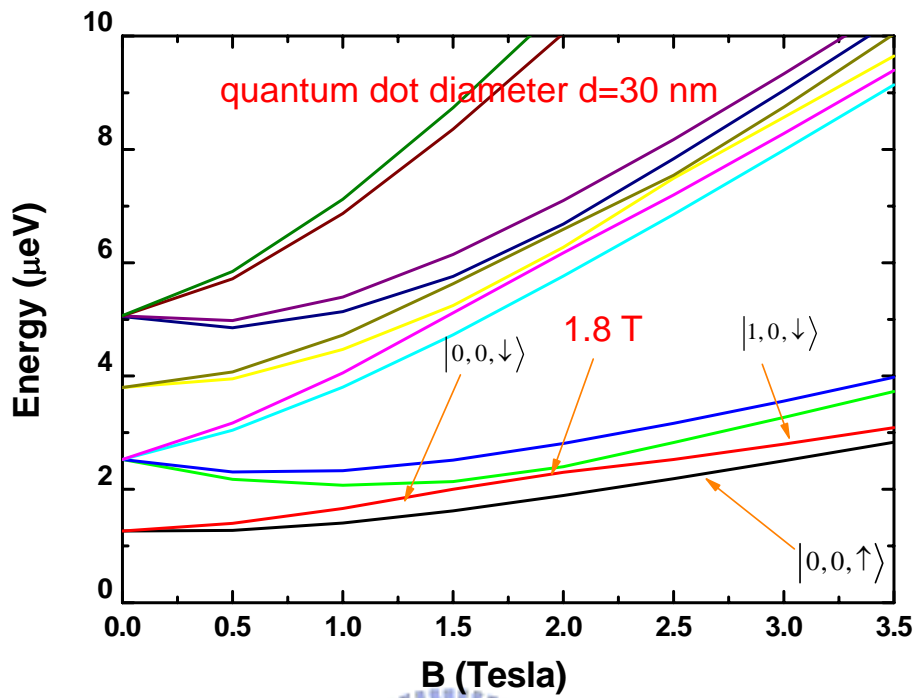


Fig.6 Energy levels for quantum dot with an effective diameter $d=30$ nm 、 $d=40$ nm, respectively with including Dressshauls effective interaction.

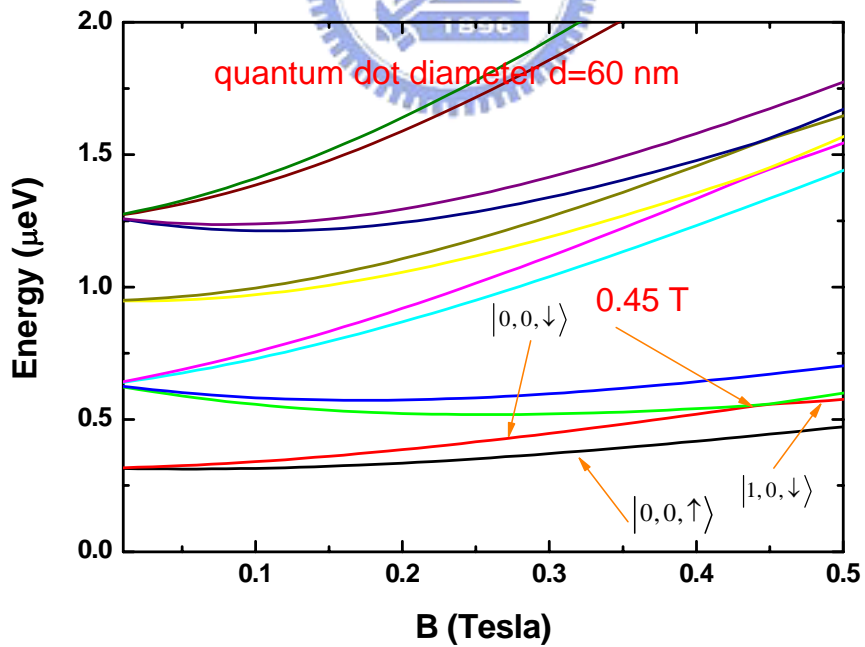
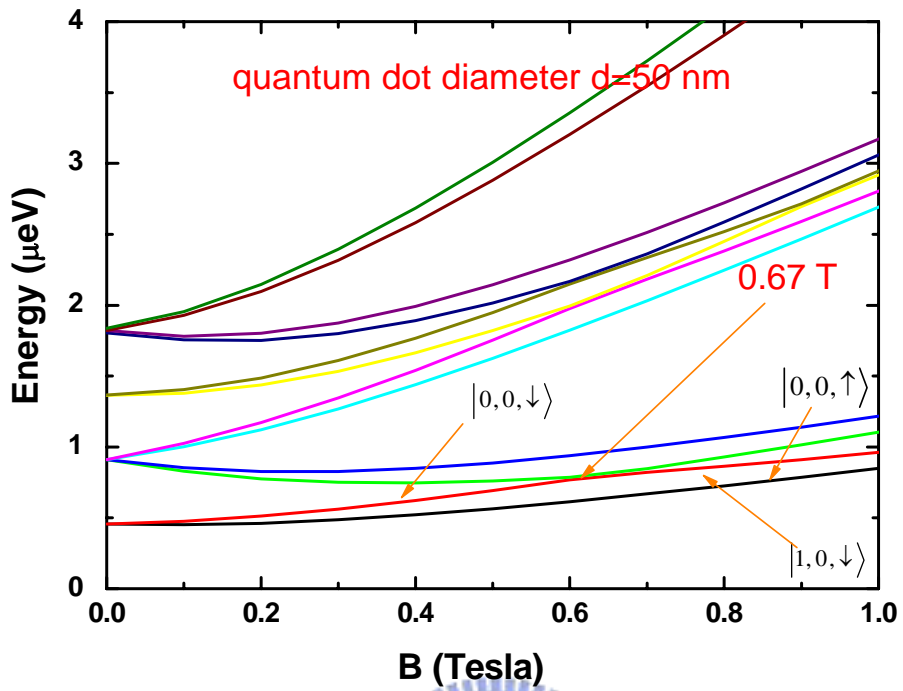


Fig.7 Energy levels for quantum dot with an effective diameter $d=50$ nm, $d=60$ nm, respectively with including Dresshauls effective interaction.

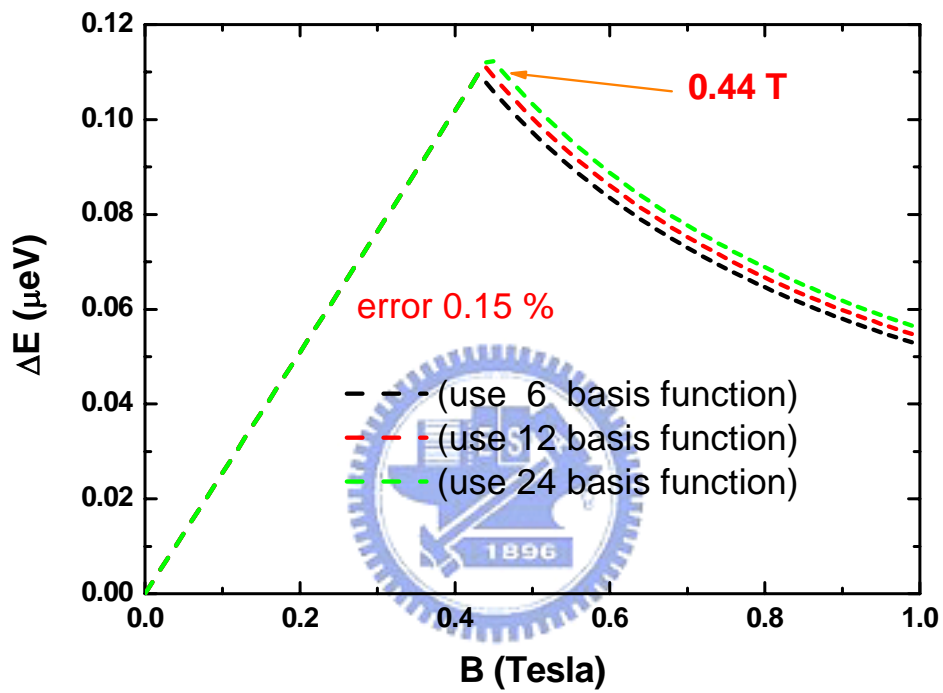


Fig.8 For $d=60\text{nm}$, 12 and 24 basis functions are included in order to obtain a convergence of the lowest 2 levels and ensure the 0.15% precision with 24 basis functions.

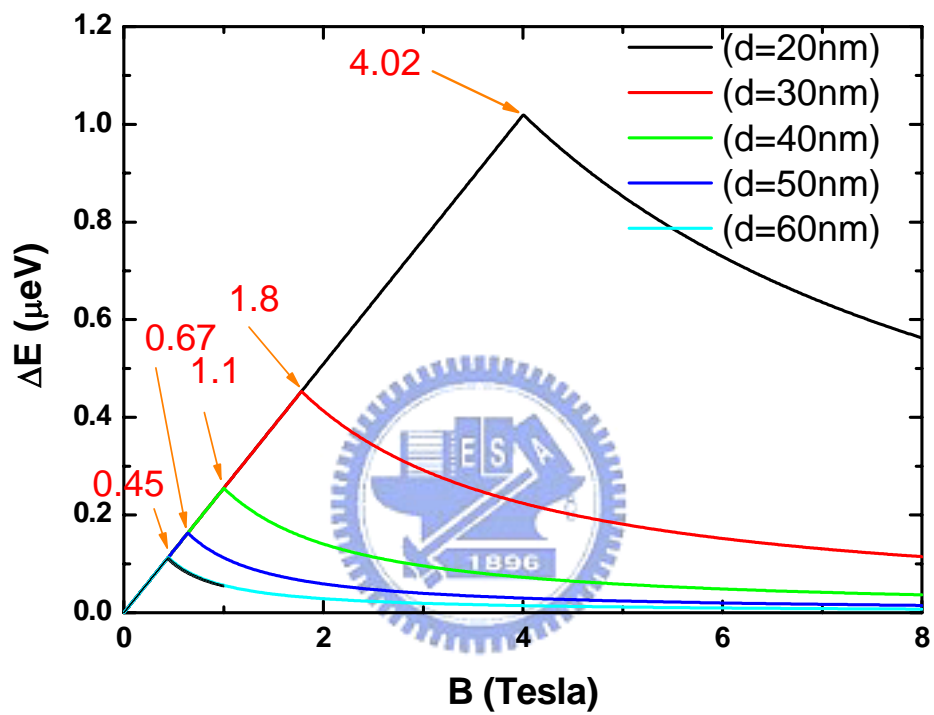


Fig.9 The corresponding energy splitting ΔE between the lowest two levels for $d=20\text{nm}$, $d=30\text{nm}$, $d=40\text{nm}$, $d=50\text{nm}$, and $d=60\text{nm}$. Anticrossing levels occur at $B=0.45\text{T}$, 0.67T , 1.1T , 1.8T , 4.02T for $d=60\text{nm}$, $d=50\text{nm}$, $d=40\text{nm}$, $d=30\text{nm}$, $d=20\text{nm}$, respectively.

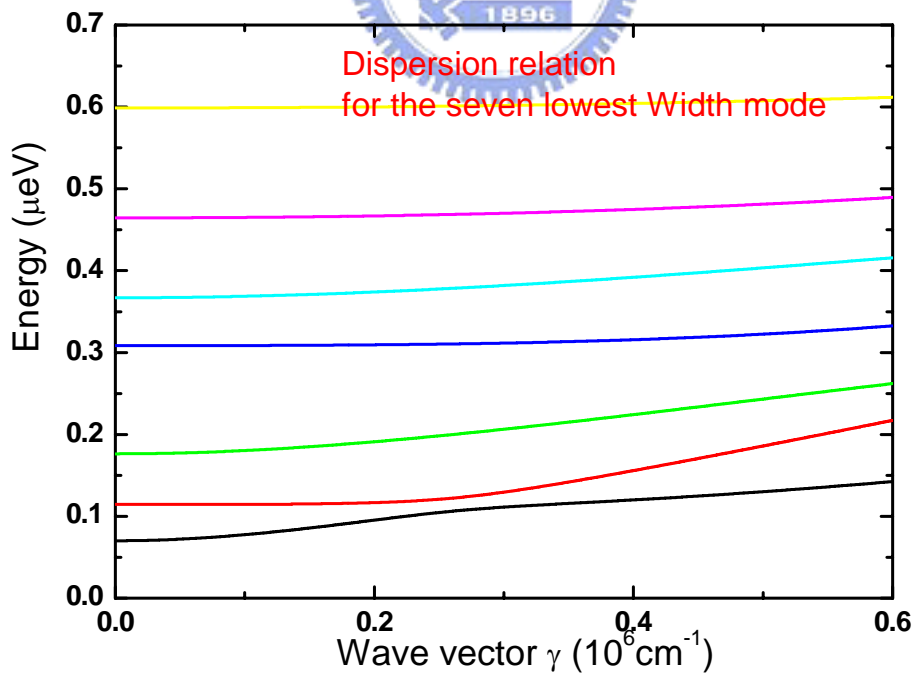
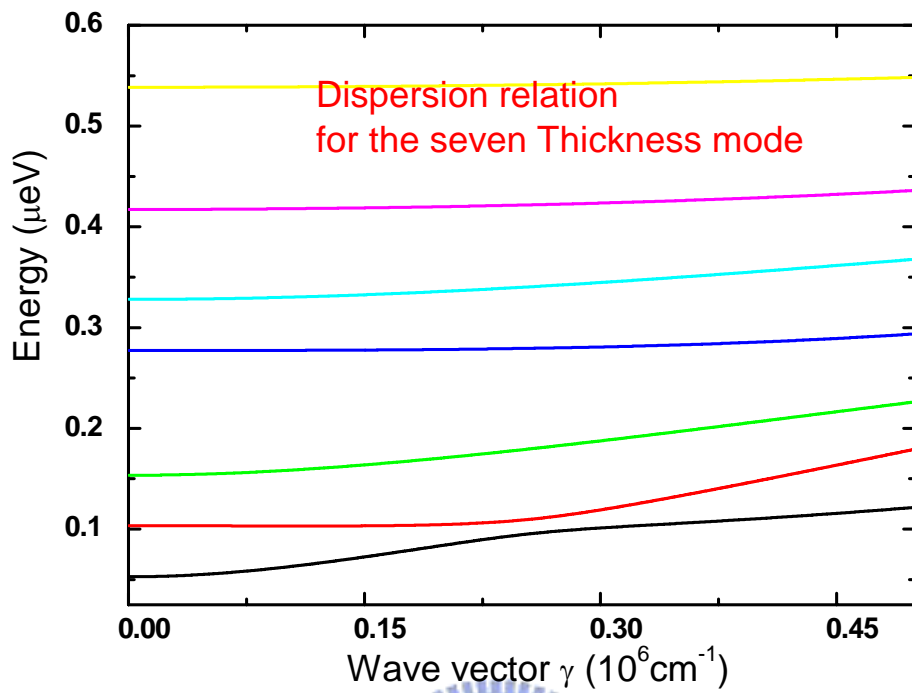


Fig.10 Dispersion curves for the six lowest width and thickness modes of a 130nmx260nm quantum wire.

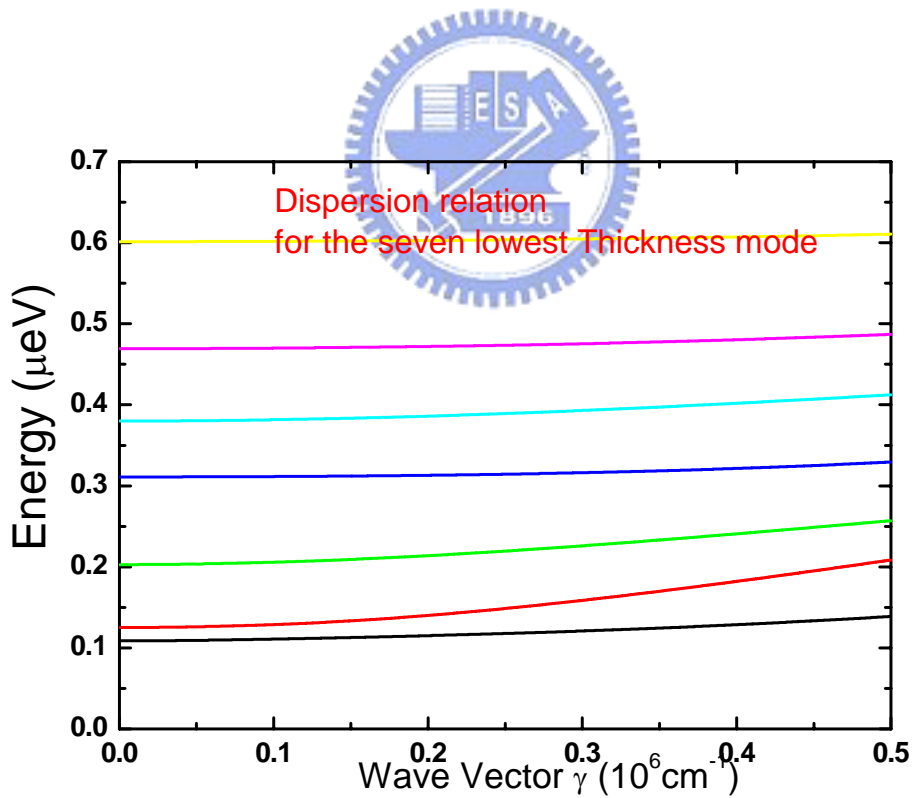
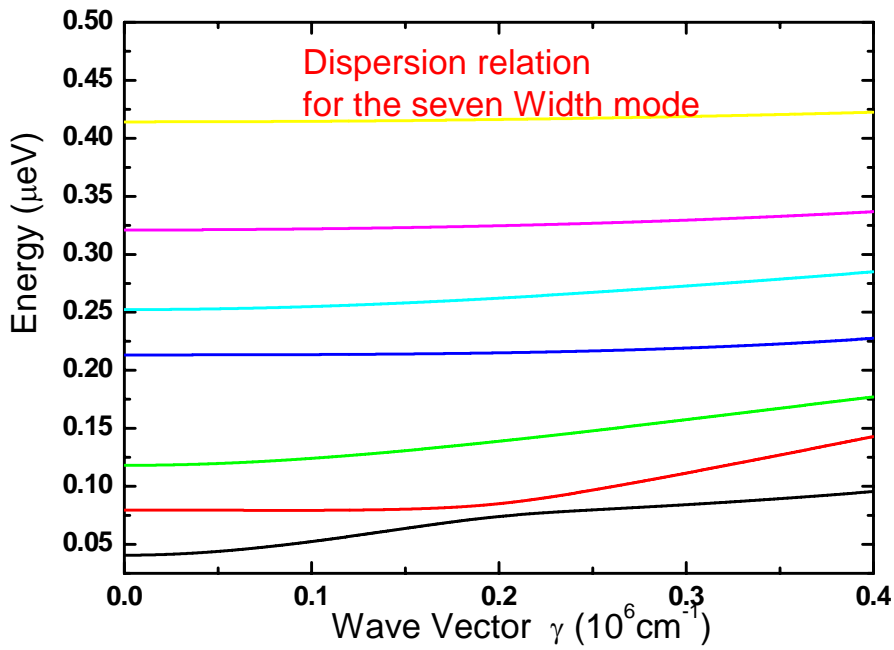


Fig.11 Dispersion curves for the six lowest width and thickness modes of a 100nmx 200nm quantum wire.

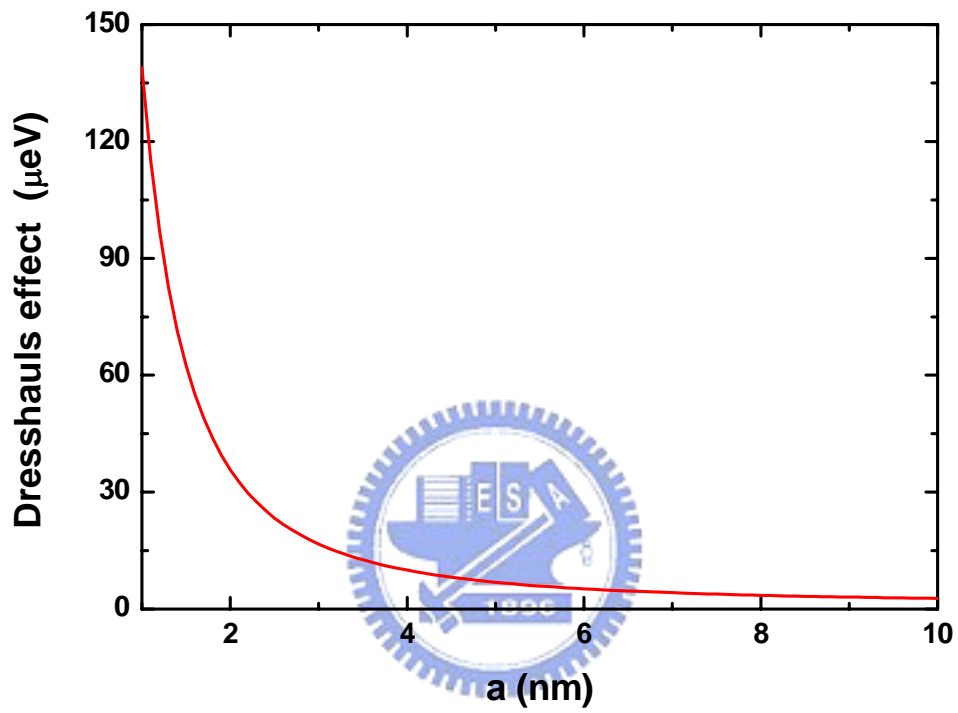


Fig.12 Magnitude effect of Dresshaus interaction for a quantum dot embedded in a quantum wire.

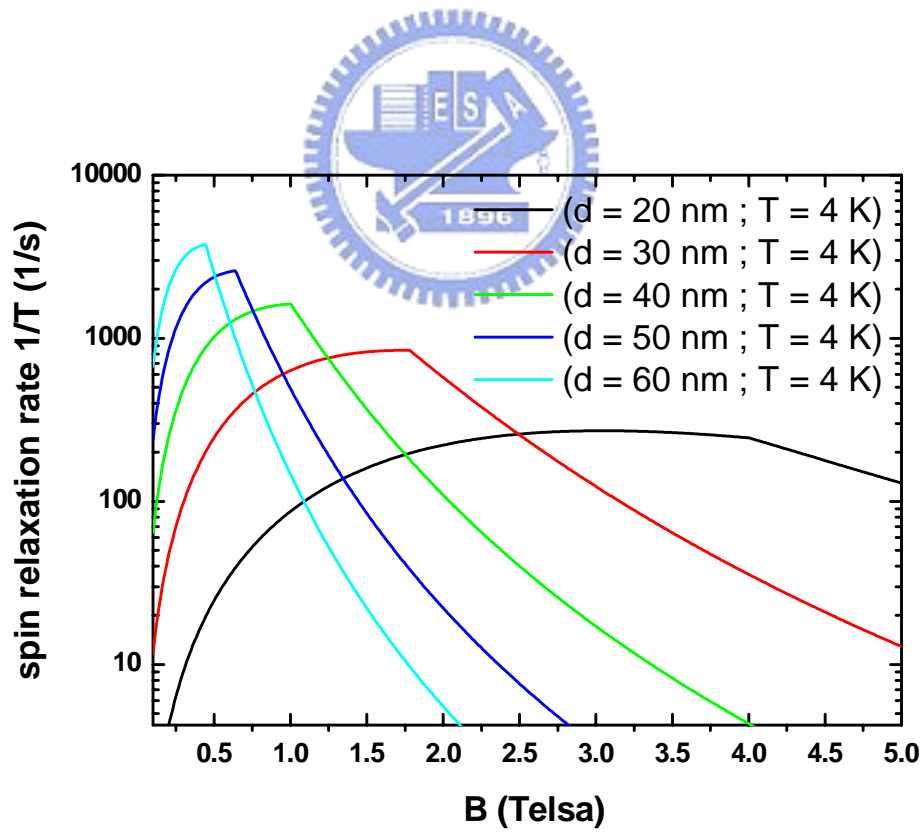
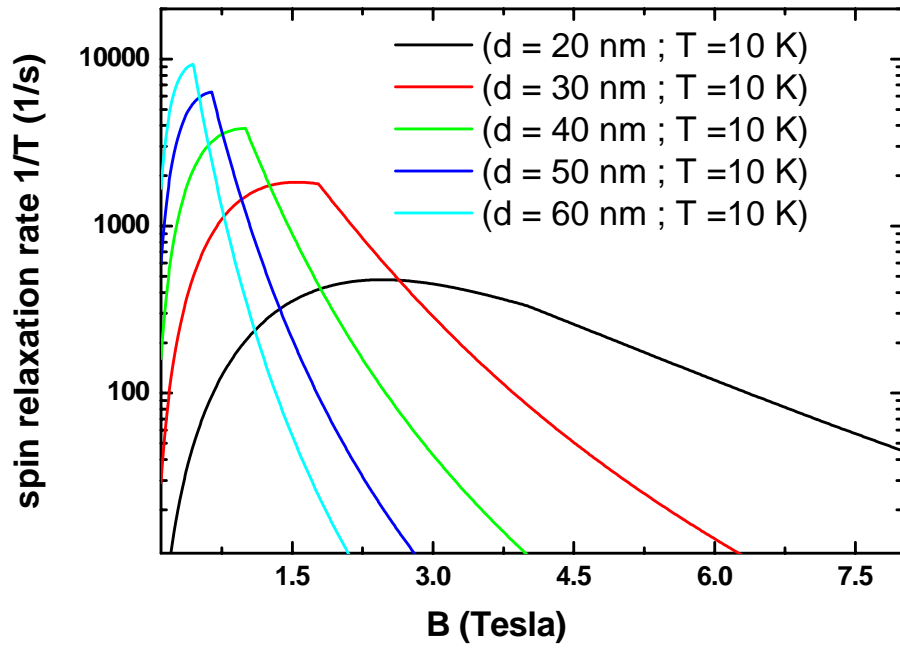


Fig.13 The spin relaxation rate versus magnetic field with the size of the quantum dot in a range of $d=20\sim d=60$ nm at temperature $T=10$ K and 4K.

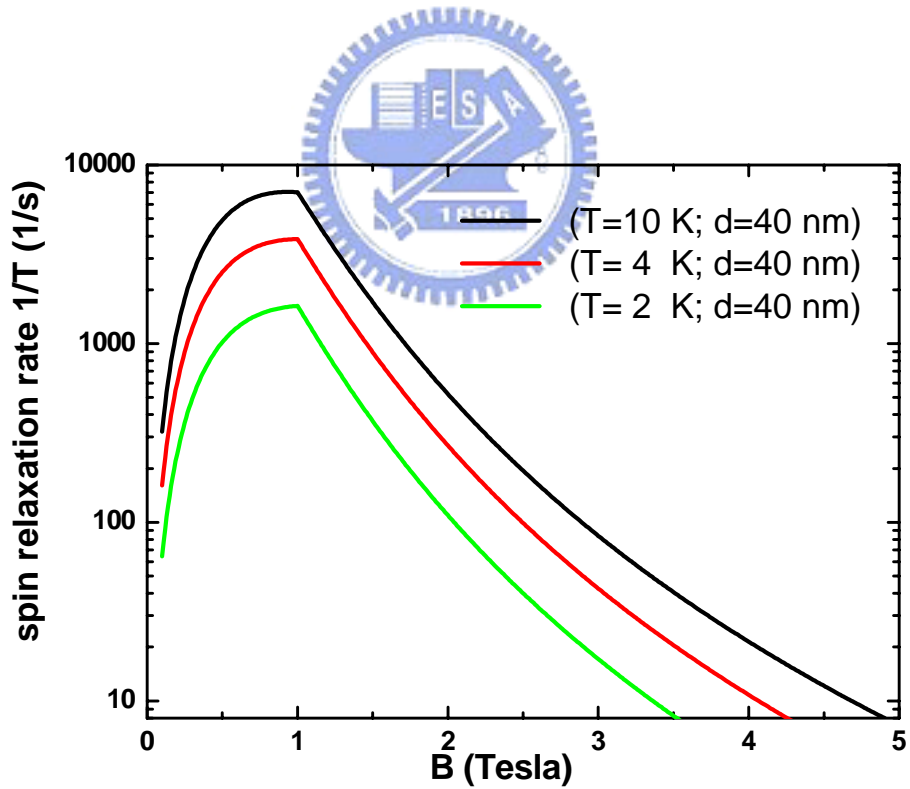
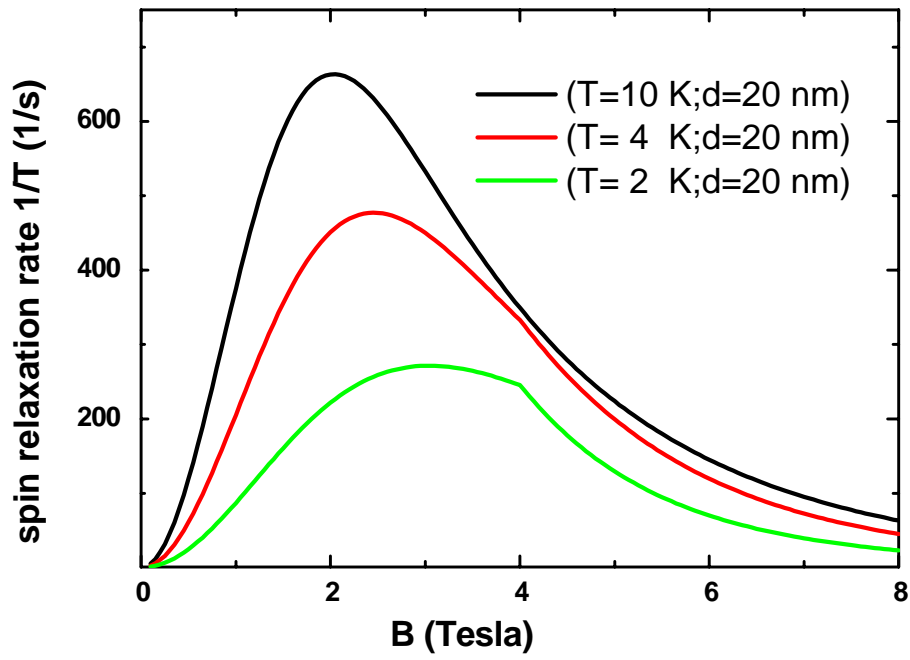


Fig.14 The spin relaxation rate versus magnetic field for various temperatures $T=10$ K 、 $T=4$ K 、 $T=2$ K and the size of the quantum dot are kept at $d=20$ 、 $d=40$ nm.

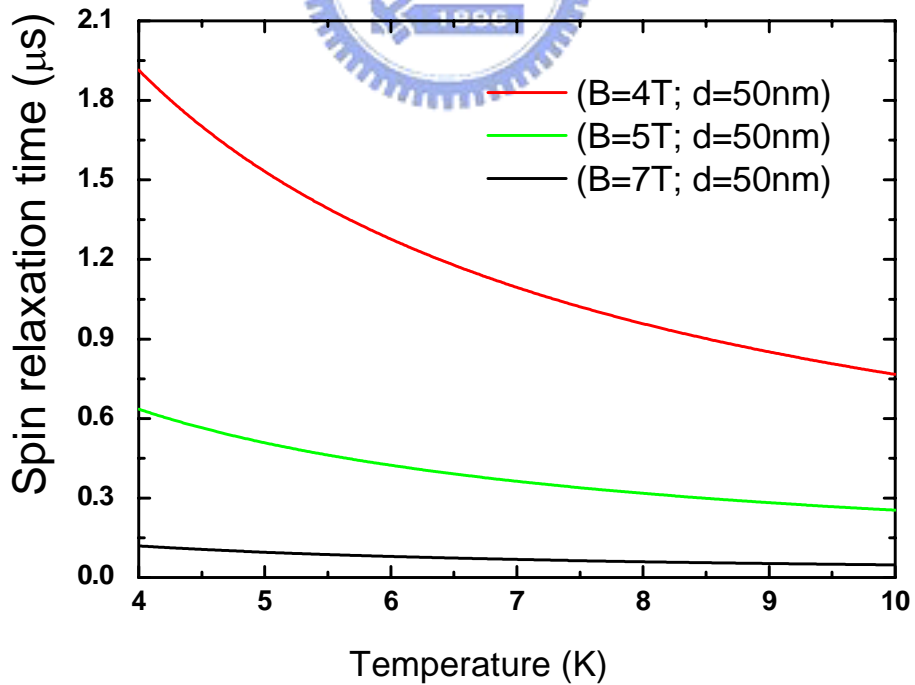
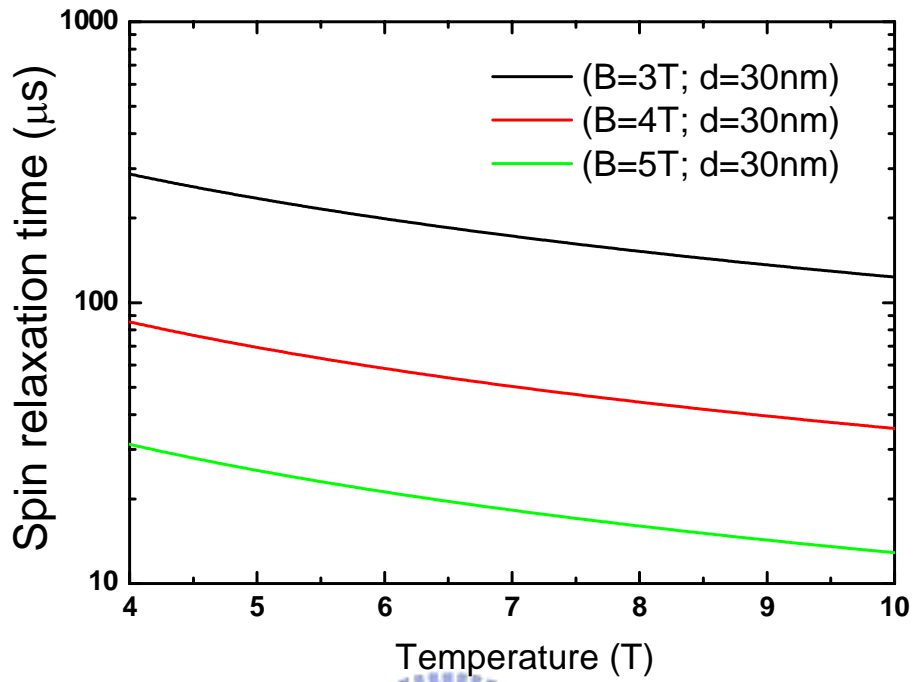


Fig.15 The spin relaxation time versus temperature under different magnetic field at $d=30\text{nm}$ and $d=50\text{nm}$.

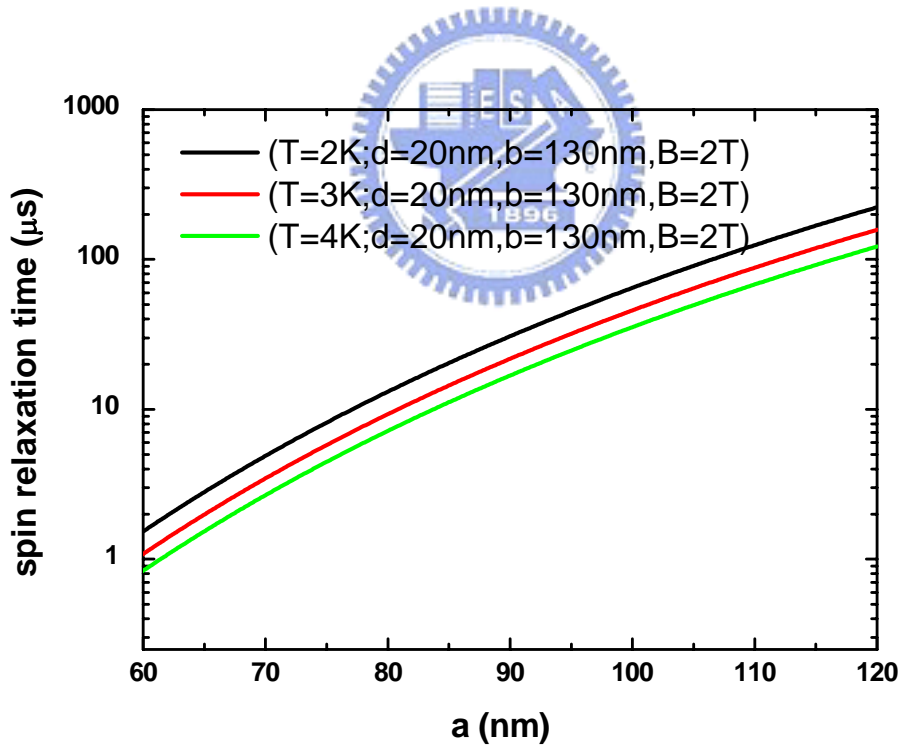
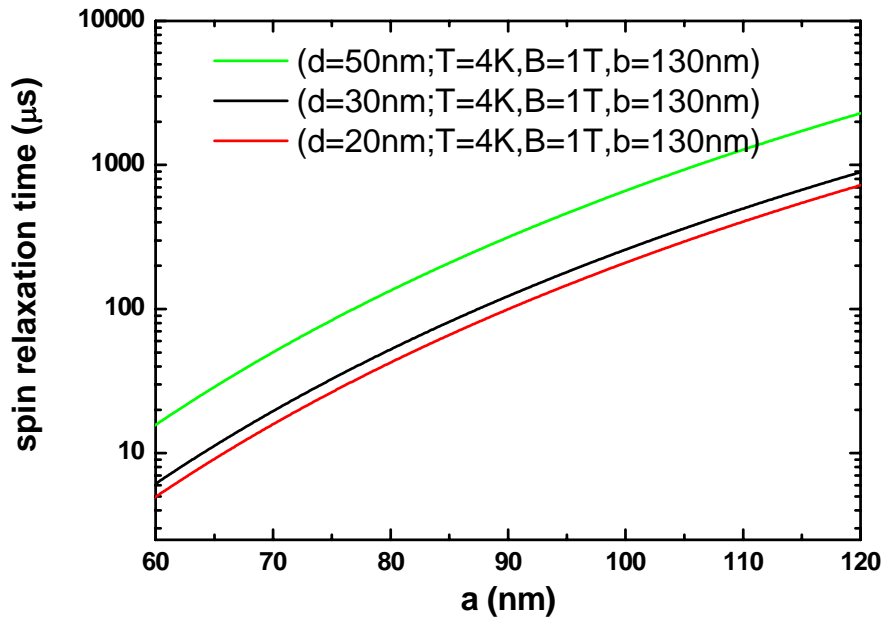


Fig.16 (a) The SRT versus the width of the quantum wire in different quantum dot diameters at $B=1\text{T}$. (b) The SRT versus the width of the quantum wire in different temperatures at $d=20\text{nm}$.

